

D. Royer (Referee)

droyer@wesleyan.edu

Received and published: 15 July 2018

Fletcher and colleagues present a Pliocene high arctic record of CO₂, temperature, plant species composition, and inferred fire frequency. They then explore how these components may be interconnected. The study summarizes an impressive amount of data. My expertise lies with paleo-CO₂ reconstruction and so my review will focus on there.

1. CO₂ reconstruction.

-Ben Fletcher developed a process-based model for paleo-CO₂ reconstruction based on the $\delta^{13}\text{C}$ of liverworts. I'm surprised that the authors have not tried to incorporate/modify this method for their own study. It's not even mentioned! Instead, the authors rely on a present-day empirical-based model, which is likely to be inferior to a process-based model. To give just one example, the authors note the problem of growth rates with other paleo-CO₂ methods (p. 15, line 10). But growth rate is a key uncertainty with the authors' method, and something that is acknowledged and (partially) addressed in the Fletcher model. This is a key deficiency with the current manuscript.

RE: We are familiar with the BRYOCARB model of Dr. Fletcher and we have incorporated it into our revised analysis. While our empirical model clearly has many errors associated with it, there are also numerous assumptions that must be made to apply a modern physiological model to a paleoenvironment in which many parameter values are hard to constrain. Nonetheless, both our empirical model and the theoretical BRYOCARB model show an increase in $\Delta^{13}\text{C}$ moss with increased partial pressure of atmospheric CO₂ as would be expected based on physical principles. However, the BRYOCARB is much less sensitive to CO₂ over the range of pCO₂ than the observed variations in samples among the elevational transects. BRYOCARB does enable us to eliminate possible explanations, such as changes in temperature and pO₂ with elevation, that have been proposed to explain the apparent decrease in $\Delta^{13}\text{C}$ of mosses with elevation. We are able to optimize variables in the BRYOCARB model to provide a plausible mean estimate of Pliocene CO₂ of 510 ppm, but the standard deviation of these estimates is extremely high ± 1080 due to the large change in pCO₂ in response to a small change in $\Delta^{13}\text{C}$ moss as predicted by the BRYOCARB model. This extremely wide range of pCO₂ estimates is still the result when unrealistically large values of $\Delta^{13}\text{C}$ (>30‰) are excluded from our Pliocene moss dataset.

Fletcher, B. J., Beerling, D. J., Royer, D. L., and Brentnall, S. J., 2005, Fossil bryophytes as recorders of ancient CO₂ levels: Experimental evidence and a Cretaceous case study: *Global Biogeochemical Cycles*, v. 19, p. GB3012, doi:10.1029/2005GB002495.

Fletcher, B. J., Brentnall, S. J., Quick, W. P., and Beerling, D. J., 2006, BRYOCARB: A process-based model of thallose liverwort carbon isotope fractionation in response to CO₂, O₂, light and temperature: *Geochimica et Cosmochimica Acta*, v. 70, p. 5676- 5691.

-Using leaf $\delta^{13}\text{C}$ to reconstruct air $\delta^{13}\text{C}$ is problematic because many factors—for example water stress—can affect leaf $\delta^{13}\text{C}$. The authors are assuming no change in water stress (and other factors that could affect leaf $\delta^{13}\text{C}$) between the present-day and Pliocene. Given what is said in section 4.3, this assumption is tenuous.

RE: We acknowledge that this is a limitation to our approach and differences in mean annual precipitation (MAP) may affect our estimates of modern $\Delta^{13}\text{C}$. However, we have controlled for this large scale variability in only sampling modern buckbean from the same boreal biome, which is much less variable than the global patterns of $\Delta^{13}\text{C}$ in response to global MAP. We also suspect that our fossil BP site was very similar to the modern Boreal forest based on our assessment of paleovegetation. This section has been updated (P7 L6-22) and the relevant Diefendorf citation has been added.

Diefendorf, A. F., Mueller, K. E., Wing, S. L., Koch, P. L., and Freeman, K. H., 2010, Global patterns in leaf ^{13}C discrimination and implications for studies of past and future climate: Proceedings of the National Academy of Sciences, USA, v. 107, p. 5738-5743.

Kohn, M. J., 2010, Carbon isotope compositions of terrestrial C_3 plants as indicators of (paleo)ecology and (paleo)climate: Proceedings of the National Academy of Sciences, USA, v. 107, p. 19691-19695.

-The empirical transfer function (Figure 3) maxes out at 360 ppm. The authors use the function to reconstruct ~450 ppm. This is a problem with extrapolation.

-The empirical transfer function is based on a mix of species. Some of the scatter is likely due to “vital effects”. This needs to be acknowledged. The best transfer function would be one based on the same species (or genus) as the fossil material.

-The authors have underestimated the uncertainty associated with their paleo- CO_2 reconstructions. As best as I can tell, their stated uncertainty (1σ , = 35 ppm) is the confidence interval from Figure 3 (dashed lines). A confidence interval says how confident one is in the regression. But if one wishes to infer the y-axis value from a new single data point (as is being done here), the prediction interval is appropriate. And the prediction interval is wider than the confidence interval. In addition, the authors have not propagated uncertainty associated with the measurement(s) of leaf $\delta^{13}\text{C}$ at each level; the authors are assuming no error. Beerling et al. (2009) lays out a solid strategy for propagating uncertainty with these kind of empirical functions.

RE: We have revised figure 3 to include the prediction interval and not the confidence interval. We have also included instrumental error with transfer function error in quadrature for our overall estimates of Pliocene CO_2 that have been updated in figure 4. We also report the mean, standard deviation and range of estimates in the revised paper.

Beerling, D. J., Fox, A., and Anderson, C. W., 2009, Quantitative uncertainty analyses of ancient atmospheric CO_2 estimates from fossil leaves: American Journal of Science, v. 309, p. 775-787.

-The authors deal with the confounding factor of water stress in the Discussion, but this section should move to the Introduction. Otherwise, the informed reader will be wondering why the authors haven't dealt with the issue while they are reading the Intro, Methods, and Results.

RE This is dealt with in the revised results, when we discuss the BRYOCARB simulations.

2. CO_2 compilation.

-The B/Ca estimates should be excluded as they are not reliable.

Allen, K. A., and Hönisch, B., 2012, The planktic foraminiferal B/Ca proxy for seawater carbonate chemistry: a critical evaluation: *Earth and Planetary Science Letters*, v. 345–348, p. 203–211.

-It looks like some Pliocene estimates have been missed. See Foster et al. (2017) for compilation and citations.

Badger, M. P. S., Schmidt, D. N., Mackensen, A., and Pancost, R. D., 2013b, High-resolution alkenone palaeobarometry indicates relatively stable pCO₂ during the Pliocene (3.3–2.8 Ma): *Philosophical Transactions of the Royal Society A*, v. 371, 20130094.

Bartoli, G., Hönisch, B., and Zeebe, R.E., 2011, Atmospheric CO₂ decline during the Pliocene intensification of Northern Hemisphere glaciations: *Paleoceanography*, v. 26, PA4213, doi:10.1029/2010PA002055.

Foster, G. L., Royer, D. L., and Lunt, D. J., 2017, Future climate forcing potentially without precedent in the last 420 million years: *Nature Communications*, v. 8, p. 14845, doi:14810.11038/ncomms14845.

Martínez-Botí, M. A., Foster, G. L., Chalk, T. B., Rohling, E. J., Sexton, P. F., Lunt, D. J., Pancost, R. D., Badger, M. P. S., and Schmidt, D. N., 2015, Plio-Pleistocene climate sensitivity evaluated using high-resolution CO₂ records: *Nature*, v. 518, p. 49–54.

Seki, O., Foster, G.L., Schmidt, D.N., Mackensen, A., Kawamura, K., and Pancost, R.D., 2010, Alkenone and boron-based Pliocene pCO₂ records: *Earth and Planetary Science Letters*, v. 292, p. 201–211.

Stap, L. B., de Boer, B., Ziegler, M., Bintanja, R., Lourens, L. J., and van de Wal, R. S. W., 2016, CO₂ over the past 5 million years: continuous simulation and new $\delta^{11}\text{B}$ - based proxy data: *Earth and Planetary Science Letters*, v. 439, p. 1–10.

Zhang, Y. G., Pagani, M., Liu, Z., Bohaty, S. M., and DeConto, R., 2013, A 40-million- year history of atmospheric CO₂: *Philosophical Transactions of the Royal Society A*, v. 371, 20130096.

RE: Thank you for bringing these more recent Pliocene paleo CO₂ reconstructions to our attention. They have been added to our compilation and Figure 1 has been revised.

3. Temperature component.

-The temperature record feels like a “third wheel” to the CO₂ and fire records. In the discussion, other temperature records (often from the same site) are emphasized more than the record generated here.

RE: The temperature record produced from the bacterial tetraethers requires less discussion than the charcoal and CO₂ because it is an existing, validated method, its results were clear, and their implication for fire etc (see below) seems straight forward. The mention of previous temperature estimates was to say they are consistent with these records – these have been removed to focus more on the GDGT results. The pollen-record suggesting a possible small-change between the

low and high charcoal components of the sequence was a simple analysis within this study, not the result of a previous study. Climate data from previous studies is only introduced for climate variables that were not measured in this study – Summer precipitation.

4. Link between fire and climate.

-Quite a lot of space in the Discussion is devoted to how fire and climate are inter- connected. And the bulk of this discussion centers on the literature. But, the record generated here shows no obvious link between fire and CO₂ or temperature (Figure 4). As a result, there is a logical disconnect. For example, from the Introduction (p. 2, lines 30-31): “We propose that fire in arctic ecosystems may also be an important proximal mechanism for amplifying arctic surface temperatures during the Pliocene.”

RE: We have attempted to clarify the importance of the ‘~13.5 °C as a key threshold for fire’ for which the GDGT’s provide evidence, through reordering of this section and some rewording of the material.. Without high enough temperatures, the fires would be much more unlikely.

However, once this threshold is crossed, differences in moisture and vegetation seem to have a larger impact on fire as suggested by charcoal deposition.

We have clarified at p. 2, lines 30-31 that the potential role of fire in Arctic amplification is part of the motivation for the study rather than a hypothesis we test.

Minor comments:

p. 3, line 15: B/Ca (not “Boron”)

RE: Corrected

p. 3, line 19: Foster et al. (2017, Nature Communications) is a more current reference

RE: This reference has been updated.

p. 3, line 24: what do you mean by “Although direct effects may be small”?

RE: Clarified in the text.

p. 4, lines 14-16: “The unit sampled spanned the 1 m remaining of Unit III as per Mitchell et al. (2016). The main sequence examined across the methods used in this study includes material above (Unit IV) and below (Unit II) Unit III, with a total sampled profile of 1.65 m.” Parts of these sentences are confusing: ‘unit’ appears to have a different meaning as ‘Unit’; what does ‘1 m remaining of Unit III’ mean? (is most of the originally sampled material gone?); the first sentence implies that all of the data come from Unit III, but the second sentence says that some of Units II and IV are included too.

RE: These sections have been edited to improve clarity

p. 6, line 31: “We also measured $\delta^{13}\text{C}$ of modern buckbean to constrain our estimates of π / pa .” More context is needed so that the reader can understand this statement. Why do the π/pa estimates need to be ‘constrained’, and why do present-day measurements allow you to do this?

RE: This section has been clarified in the revised version (P7 L1-10)

p. 6, line 32: say that cellulose was measured (ditto in line 31).

RE: The suggested changes have been made.

p. 7, line 11: “paleosols”

RE: The suggested change has been made.

p. 7, lines 30-32: Provide a citation for the transfer function. Is the combined error a one-sigma error? Two-sigma? Was quadrature used to calculate the combined error?

RE: See explanation for the comment of referee #1. We don’t use this.

p. 8, line 19: “MAT”?

RE: The suggested change has been made.

p. 9, lines 17-18: What is the difference between a maximum probability age and an optimized age?

RE: We have deleted reference to the optimized age as the Bayesian most probable age is now most frequently used.

p. 9, line 22: Unweighted mean age already stated. p. 9, line 23: How was this uncertainty computed?

RE: This section has now been reworded for clarity in response to reviewer 1.

p. 9, lines 28-30: The first and second parts of this sentence are saying the same thing.

RE: This section has been edited.

p. 9, lines 30-31: I don’t understand why nonlinearity is expected because Figure 3 plots the log of carbon isotope discrimination (also, see next sentence in the manuscript).

RE: A linear model is now applied in the revised manuscript.

p. 10, line 2: These “other processes” don’t need to be nonlinear; the combined additive effect is nonlinear.

RE: A linear model is now applied in the revised manuscript.

p. 10, lines 9-12: It is inappropriate to use the site-specific regression because the associated site-specific information is not available for the Pliocene samples.

RE: This section has been edited.

p. 10, line 11: Is this the same model as in line 1?

RE: This section has been edited as a linear model is now applied in the revised manuscript.

p. 15, line 23: “over the Pliocene”. Surely you don’t mean the entire Pliocene?

RE: This has now been edited for clarity ‘over the deposition of this sediment during the Pliocene’

p. 19, lines 30-31: “fire played an active role in influencing the climate of the Arctic during the Pliocene.” That’s not what your data suggest (Figure 4).

RE: It is true that the apparent change in fire frequency at our site did not result in a change in a respective change in climate. This section has been edited to better reflect our results – that a change in fire seems to drive a change in environment, and that in the similar modern boreal system this has impacts on the Earth’s radiative budget.

Figure 3: Please add the theoretical regression (from equations 2 & 3). Add linear y-axis tick marks too. In the caption, say that the isotopic discrimination is based on cellulose (or an inferred cellulose value).

RE: This figure has been revised to include theoretical fit from BRYOCARB along with our empirical fit to observations. Scale is now linear based on comments from Smittenberg (above) and y-ticks are included. Caption has been revised stating that all values normalized to cellulose.

Figure 4: unit needed for x-axis.

RE: The suggested change has been made.

Figure S2: Plots need axis labels

RE: Figure S2 has been revised, and now has clear axis labels

Figure S3: Axis and tick mark labels are too pixelated to read

RE: A higher resolution version of this figure is available.

References

- Farquhar, G. D., J. R. Ehleringer & K. T. Hubick (1989) Carbon isotope discrimination and photosynthesis. *Annual review of plant biology*, 40, 503-537.
- Fletcher, B. J., S. J. Brentnall, C. W. Anderson, R. A. Berner & D. J. Beerling (2008) Atmospheric carbon dioxide linked with Mesozoic and early Cenozoic climate change. *Nature Geoscience*, 1, 43-48.
- Pagani, M., Z. Liu, J. LaRiviere & A. C. Ravelo (2010) High Earth-system climate sensitivity determined from Pliocene carbon dioxide concentrations. *Nature Geoscience*, 3, 27-30.
- Ravelo, A. C., D. H. Andreasen, M. Lyle, A. Olivarez Lyle & M. W. Wara (2004) Regional climate shifts caused by gradual global cooling in the Pliocene epoch. *Nature*, 429, 263-267.
- Skrzypek, G., A. Kałużny, B. Wojtuń & M.-O. Jędrysek (2007) The carbon stable isotopic composition of mosses: a record of temperature variation. *Organic geochemistry*, 38, 1770-1781.
- White, J., P. Ciais, R. Figge, R. Kenny & V. Markgraf (1994) A high-resolution record of atmospheric CO₂ content from carbon isotopes in peat. *Nature*, 367, 153 - 156.

Elevated atmospheric CO₂ and fire linked to arctic amplification of temperature during the Early to mid-Pliocene

Tamara Fletcher^{1*}, Lisa Warden^{2*}, Jaap S. Sinninghe Damsté^{2,3}, Kendrick J. Brown^{4,5}, Natalia Rybczynski^{6,7}, John Gosse⁸, and Ashley P Ballantyne¹

¹ College of Forestry and Conservation, University of Montana, Missoula, 59812, USA

² Department of Marine Microbiology and Biogeochemistry, NIOZ Royal Netherlands Institute for Sea Research, Den Berg, 1790, Netherlands

³ Department of Earth Sciences, University of Utrecht, Utrecht, 3508, Netherlands

⁴ Natural Resources Canada, Canadian Forest Service, Victoria, V8Z 1M, Canada

⁵ Department of Earth, Environmental and Geographic Science, University of British Columbia Okanagan, Kelowna, V1V 1V7, Canada

⁶ Department of Palaeobiology, Canadian Museum of Nature, Ottawa, K1P 6P4, Canada

⁷ Department of Biology & Department of Earth Sciences, Carleton University, Ottawa, K1S 5B6, Canada

⁸ Department of Earth Sciences, Dalhousie University, Halifax, B3H 4R2, Canada

*Authors contributed equally to this work

Correspondence to: Tamara Fletcher (tamara.fletcher@umontana.edu)

Abstract. The mid-Pliocene is a valuable time interval for understanding the mechanisms that determine equilibrium climate at current atmospheric CO₂ concentrations. One intriguing, but not fully understood, feature of the early to mid-Pliocene climate is the amplified arctic temperature response. Current models underestimate the degree of warming in the Pliocene Arctic and validation of proposed feedbacks is limited by scarce terrestrial records of climate and environment, as well as discrepancies in current CO₂ proxy reconstructions. Here we reconstruct the CO₂ summer temperature and fire regime from a sub-fossil fen-peat deposit on west-central Ellesmere Island, Canada, that has been chronologically constrained using radionuclide dating to 3.9 ± 1.5/-0.5 Ma.

An empirical transfer function was derived and applied to carbon isotopic measurements of paleo mosses to yield an estimate of Pliocene mean atmospheric CO₂ concentrations of 410 ± 50 ppm, which are slightly lower than theoretical model predictions of 510 ppm. The estimate for average mean summer temperature is 15.4 ± 0.8°C using specific bacterial membrane lipids, i.e. branched glycerol dialkyl glycerol tetraethers. Macro-charcoal was present in all samples from this Pliocene section with notably higher charcoal concentration in the upper part of the sequence. This change in charcoal was synchronous with a change in vegetation that saw fire promoting taxa increase in abundance. Paleovegetation reconstructions are consistent with warm summer temperatures, relatively low summer precipitation and an incidence of fire comparable to fire adapted boreal forests of North America, or potentially central Siberia.

To our knowledge, this study represents the northern-most evidence of fire in Earth's history and highlights the important role of forest fire in the ecology and climatic processes of the Pliocene High Arctic. The results provide evidence that terrestrial fossil localities in the Pliocene High Arctic were probably formed during warm intervals that coincided with relatively high CO₂ concentrations that supported productive biotic communities. This study indicates that interactions between paleovegetation and paleoclimate were mediated by fire in the High Arctic during the Pliocene, even though CO₂ concentrations were similar to modern.

Formatted: Left: 25.4 mm, Right: 25.4 mm, Top: 25.4 mm, Bottom: 25.4 mm, Width: 215.9 mm, Height: 279.4 mm, Header distance from edge: 12.7 mm, Footer distance from edge: 12.7 mm, From text: 0 mm

Deleted: The role of e

Deleted: increased

Deleted: in

Deleted: A

Deleted: and

Deleted: re-dated 3.9 ± 1.5/-0.5 Ma

Deleted: and investigate fire as a potential feedback to Arctic amplification of warming during the mid-Pliocene. ¶

Deleted: Average CO₂ was determined using isotope ratios of mosses to be 440 ± 50 ppm

Deleted: furthest

Deleted: fire during the Pliocene

Deleted: only ~30 ppm higher than

1 Introduction

Current rates of warming in the Arctic are almost double the rate of global warming. Since 1850, global land surface temperatures have increased by approximately 1.0°C, whereas arctic surface land temperatures have increased by 2.0°C (Jones and Moberg, 2003; Pagani et al., 2010; Francis and Skiffington, 2015). Such arctic amplification of temperatures has also occurred during other warm climate anomalies in Earth's past. Paleoclimate records from the Arctic indicate that the change in arctic summer temperatures during past global warm periods was 3–4 times larger than global temperature change (Miller et al., 2010). While the latest ensemble of earth system models (ESMs) provide fairly accurate predictions of the modern amplification of arctic temperatures hitherto observed (Marshall et al., 2014), they often under-predict the amplification of arctic temperatures during past warm intervals in Earth's history, including the Eocene (33.9–56 Ma; Huber, 2008; Shellito et al., 2009), and the Pliocene (2.6–5.3 Ma; Dowsett et al., 2012; Salzmann et al., 2013) epochs. These differences suggest that either the models are not simulating the full array of feedback mechanisms properly for past climates, or that the full array of fast and slow feedback mechanisms have not fully engaged for the modern Arctic. If the later, the Arctic region has yet to reach the full amplification potential demonstrated in the past.

The Pliocene is an intriguing climatic interval that may offer important insights into climate feedbacks. Atmospheric CO₂ values varied (Royer et al., 2007) decreasing from values comparable to modern (Haywood et al., 2016; Pagani et al., 2010; Stap et al., 2016), to lower levels (Raymo et al., 2006); a state transition that may revert in the future under high CO₂. Of additional importance, continental configurations were similar to present (Dowsett et al., 2016). While global mean annual temperatures (MATs) during the Pliocene were only ~3°C warmer than present day (Fig. 1), arctic land surface MATs may have been as much as 15 to 20°C warmer (Ballantyne et al., 2010; Csank et al., 2011a; Csank et al., 2011b; Fletcher et al., 2017). Further, arctic sea surface temperatures may have been as much as 10 to 15°C warmer than modern (Robinson, 2009), and sea-levels were approximately 25m higher than present (Dowsett et al., 2016). As such, the terrestrial environment of the Arctic was significantly different, with tree line ecosystems at much higher latitudes nearly eliminating the tundra biome (Salzmann et al., 2008).

Several mechanisms have been proposed as drivers of arctic amplification, including vastly reduced sea-ice extent (Ballantyne et al., 2013), cloud and atmospheric water vapor effects (e.g. Feng et al., 2016; Swann et al., 2010), vegetation controls on albedo (Otto-Bliesner and Upchurch Jr, 1997), and increased meridional heat transport by the oceans (Dowsett et al., 1992) though it is now considered to be of lesser influence (Hwang et al., 2011). We propose that fire in arctic ecosystems may also be an important mechanism for amplifying arctic surface temperatures during the Pliocene, and so seek to understand its characteristics through quantification from the sediment record.

Although it is generally thought that atmospheric CO₂ concentrations of ~400 ppm provided the dominant global radiative forcing during the mid-Pliocene, CO₂ proxies over the Pliocene do not all agree (Fig. 1). Reconstructions of Pliocene CO₂ range between 190 and 440 ppm (Martinez-Boti et al., 2015; Seki et al., 2010). While CO₂ estimates from stomata and paleosols tend to be less precise, they are within the range of boron and alkenone derived estimates (Royer, 2006; Foster et al. 2017). Thus, there is no clear consensus on CO₂ concentrations in Earth's atmosphere during the Pliocene. Dating uncertainties are an additional confounding factor complicating site to site comparisons. Although modelled direct effects of this level of CO₂ variation may be small (Feng et al., 2017), reconstructing the

Deleted: ,

Deleted: #1834}

Deleted: It captures the transition from the preceding Miocene to the Pleistocene when orbital regulators of climate transitioned from the 41,000 year obliquity cycle to the 100,000 year eccentricity cycle, respectively.

Deleted: likewise

Deleted: proximal

Deleted: necessarily

Deleted: Overall, r

Deleted: For example, Boron-based Pliocene CO₂ reconstructions (258 ± 35 ppm; mean ± s.d.; Tripati et al., 2009) tend to be lower than (258 ± 35 ppm; mean ± s.d.; Tripati et al., 2009), the alkenone-based isotopic proxy average 357 ± 45 ppm (Pagani et al., 2010; Seki et al., 2010), whereas other estimates suggest values between 330–400 ppm (Seki et al., 2010).

Moved (insertion) [1]

Moved up [1]: (258 ± 35 ppm; mean ± s.d.; Tripati et al., 2009)

Deleted: , further

Deleted: This suggests an additional hypothesis to explain why modern Arctic amplification and models agree, but the Pliocene amplification estimates and models disagree; that CO₂ levels were higher than currently used for model boundary conditions during the deposition of the proxies used for past temperature estimation at sites with high dating uncertainties.

CO₂ from the same deposits from which paleoclimate and paleoecological proxies are derived, may help reconcile previous estimates and contribute to constraining climate sensitivities during the Pliocene.

To advance [our](#) understanding of arctic amplification during past warm intervals in Earth's history such as the Pliocene this investigation targets an exceptionally well-preserved arctic sedimentary sequence to simultaneously reconstruct atmospheric CO₂, summer temperature, vegetation and fire [from a single site](#).

Deleted: disturbance history

Deleted: over its deposition

2 Methods

2.1 Site description

To investigate the environment and climate of the Pliocene Arctic we focused on [the](#) Beaver pond (BP) [fossil site](#), located at 78° 33' N (Fig. 2) on Ellesmere Island. The stratigraphic section located at ~380 meters above sea level (MASL) today includes unconsolidated bedded sands and gravels, and rich organic layers including a thick fossil rich peat layer, up to 2.4 m thick, with sticks gnawed by an extinct beaver (*Dipoides spp.*). The assemblage of fossil plants and animals at BP has been studied extensively to gain insight into the past climate and ecology of the Canadian High Arctic (Ballantyne et al., 2006; Csank et al., 2011a; Csank et al., 2011b; Fletcher et al., 2017; Mitchell et al., 2016; Rybczynski et al., 2013; Tedford and Harington, 2003; Wang et al., 2017). Previous paleoenvironmental evidence suggests the main peat unit is a rich fen deposit with a neutral to alkaline pH, associated with open water (Mitchell et al., 2016), likely a lake edge fen or shallow lake fen, within a larch-dominated forest-tundra environment (Matthews and Fyles, 2000), not a low pH peat-bog. While the larch species identified at the site, *Larix groenlandia*, is extinct (Matthews and Fyles, 2000), many other plant remains are Pliocene examples of taxa that are extant (Fletcher et al., 2017).

Deleted: a fossil site,

The fen-peat unit examined in this study was sampled in 2006 and 2010. [The main sequence examined across the methods used in this study includes material from Unit II, the entire span of Unit III, and material from Unit IV per Mitchell et al. \(2016\)](#), with a total sampled profile of 1.65 m. Unit III has been estimated to represent ~20 000 years of deposition based on modern northern fen growth rates (Mitchell et al., 2016). The atmospheric CO₂ estimates from this locality were based on 22 sample layers from the 2006 field campaign, and the charcoal was based on 31, while the temperature estimates from specific bacterial membrane lipids were taken from 22 of the sample layers collected in 2006 and an additional 12 samples collected in 2010. The same samples from the 2006 season were analyzed for each of CO₂, mean summer temperature and char count where contents of the sample allowed. Pollen was tabulated [from](#) 10 samples [from the](#) 2006 [sequence](#), located at different stratigraphic depths.

Deleted: The unit sampled spanned the 1 m remaining of Unit III as per Mitchell et al. (2016).

Deleted: above (Unit IV) and below (Unit II) Unit III

Deleted: in

Deleted: of

Deleted: se

2.2 Geochronology

While direct dating of the peat was not possible, we were able to establish a burial age for fluvial sediments deposited approximately 4–5 m above and 30 m to the southwest of the peat. We used a method based on the ratio of isotopes produced in quartz by secondary cosmic rays. The cosmogenic nuclide burial dating approach measures the ratio of cosmogenic ²⁶Al ($t_{1/2} = 0.71$ Ma) and ¹⁰Be ($t_{1/2} = 1.38$ Ma) in quartz sand grains that were exposed on hillslopes and alluvium prior to final deposition at BP. Once the quartz grains are completely shielded from cosmic rays, the ratio of

the pair will predictably decrease because ^{26}Al has double the radiodecay rate of ^{10}Be . In 2008, four of the medium to coarse grained quartz samples were collected from a vertical profile of planar crossbedded fluvial sands between 8.7 and 10.4 m below the overlying till surface. The samples were 5 cm thick, separated by an average of 62 cm, and should closely date the peat (the sandy braided stream beds represent on the order of $\sim 10^4$ years from the top of the peat to the highest sample). Quartz concentrates were extracted from the arkosic sediment using Frantz magnetic separation, heavy liquids, and differential leaching with HF in ultrasonic baths. When sample aliquots reached aluminum concentrations <100 ppm (ICP-OES) as a proxy of feldspar abundance, the quartz concentrate was subjected to a series of HF digestion and rinsing steps to ensure that more than 30% of the quartz had been dissolved to remove meteoric ^{10}Be . Approximately 200 mg of Be extracted from a Homestake Gold Mine beryl-based carrier was added to 150 g of each quartz concentrate (no Al carrier was needed for these samples). Such large quartz masses were digested because of the uncertainty in the abundance of the faster decaying isotope. Following repeated perchloric-acid dry-downs to remove unreacted HF, pH-controlled precipitation, column chemistry ion chromatography to extract the Be and Al ions, precipitation in ultrapure ammonia gas, and calcination at temperatures above 1000°C in a Bunsen flame for three minutes, oxides were mixed with equal amounts of niobium and silver by volume. These were packed into stainless steel targets for measurement at Lawrence Livermore National Laboratory's accelerator mass spectrometer (AMS). Uncertainty estimates for $^{26}\text{Al}/^{10}\text{Be}$ were calculated as 1σ by combining AMS precision with geochemistry errors in quadrature. For a complete detailed description of TCN methods see Rybczynski et al. (2013). The ages provided here are updated from Rybczynski et al. (2013) by using more recent production rate information and considering the potential for increasing exposure to deeply penetrating muons during the natural post-burial exhumation at BP.

2.3 Atmospheric CO_2 Reconstruction

In order to reconstruct atmospheric CO_2 concentrations during the Pliocene, we derived a method based on the different sensitivity of isotopic discrimination of plant groups to their environment (Farquhar et al., 1989; Fletcher et al., 2008; White et al., 1994). Specifically, we used measurements of stable carbon isotopic discrimination in C_3 vegetation to approximate the carbon isotopic signature of the atmosphere, and measurements of carbon isotopic discrimination in bryophytes to estimate the partial pressure of atmospheric CO_2 , which was then converted to atmospheric CO_2 concentration. According to theory (Farquhar et al., 1989), plants discriminate ($\Delta^{13}\text{C}$) against the heavier isotope in atmospheric CO_2 , such that:

$$\Delta^{13}\text{C} = a + (b - a) \frac{p_i}{p_a} \quad (1)$$

where the fractionations of atmospheric CO_2 due to diffusion ($a \sim -4.4\text{‰}$) and carboxylation by the enzyme rubisco ($b \sim -27\text{‰}$) are constraints. Thus, isotopic fractionation in C_3 plants ($\Delta^{13}\text{C}_{\text{C}_3}$) is largely a function of stomatal control of partial pressure of intercellular CO_2 (p_i) with respect to the partial pressure of atmospheric CO_2 (p_a). However, bryophytes lack stomata and thus a mechanism for actively regulating p_i , such that isotopic fractionation ($\Delta^{13}\text{C}_{\text{bryo}}$) varies mainly as a function of partial pressure in atmospheric CO_2 (i.e. p_a). While other environmental factors,

Formatted: Superscript

Deleted: .00

Deleted: .00

Deleted: W

Deleted: a is

Deleted: b is the fractionation of atmospheric CO_2 due to

Deleted: This physical and chemical discrimination is then modulated by stomatal control of partial pressure of intercellular CO_2 (p_i) with respect to the partial pressure of atmospheric CO_2 (p_a). Therefore isotopic discrimination

Deleted: conductance and in

Deleted: that

Deleted: ($\Delta^{13}\text{C}_{\text{bryo}}$) is largely a

such as humidity, temperature, light availability, and microclimate [may](#) also play important roles in isotopic discrimination in bryophytes (Fletcher et al., 2008; Ménot and Burns, 2001; Royles et al., 2014; Skrzypek et al., 2007; Waite and Sack, 2011; White et al., 1994), the first order control on discrimination is the partial pressure of atmospheric CO₂ (Fletcher et al., 2008; White et al., 1994). Because atmospheric CO₂ is relatively well mixed in the troposphere its mean annual concentration does not [differ significantly by location](#). However, because total atmospheric pressure decreases with [atmospheric height \(h\)](#), the partial pressure of atmospheric CO₂ must also decrease according to the following exponential function:

$$p_{a(h)} = p_{a(i)} e^{-h/H} \quad (2)$$

[such that the partial pressure of atmospheric CO₂ at any given height in the atmosphere \(\$p_{a\(h\)}\$ \) can be calculated based on the initial atmospheric partial pressure of atmospheric CO₂ \(\$p_{a\(i\)}\$ \) and a reference height \(\$H = 7600\$ m\), where atmospheric pressure goes to 0.37 Pa \(Bonan, 2015\). Therefore assuming that carbon isotopic discrimination in bryophytes varies in response to the partial pressure of atmospheric CO₂ \[we can predict from basic physical principles an increase in \\$\Delta^{13}\text{C}_{\text{bryo}}\\$ in response to an increase in \\$p_{a\\(h\\)}\\$\]\(#\) . Furthermore, if the assumptions of this empirical relationship are valid, then this empirical relationship can in theory be used to predict the partial pressure of atmospheric CO₂ based on carbon isotopic measurements of bryophytes.](#)

To test this prediction, we compiled data from four studies investigating carbon isotopic variability of different bryophytes, primarily mosses, along elevational transects at different locations. Based on the elevations [and locations of moss samples](#), the atmospheric partial pressure of atmospheric CO₂ was estimated from ERA-interim reanalysis data of total atmospheric pressure (Dee et al., 2011) in conjunction with globally averaged atmospheric CO₂ concentrations (Global View-CO₂, 2013) [from the years moss samples were collected](#). For our analysis we only included measurements of carbon isotopic variability in non-vascular mosses and all isotopic values were normalized to cellulose based on the empirical relationship reported by Ménot and Burns (2001). Carbon isotopic discrimination values for all plant material was calculated as:

$$\Delta^{13}\text{C} = (\delta^{13}\text{C}_{\text{atm}} - \delta^{13}\text{C}_{\text{plant}}) / (1 + \delta^{13}\text{C}_{\text{plant}}/1000) \quad (3)$$

where $\delta^{13}\text{C}_{\text{plant}}$ represents the C isotopic composition of plant cellulose and $\delta^{13}\text{C}_{\text{atm}}$ represents the mean annual carbon isotopic composition of atmospheric CO₂ of the year when samples were collected (Global View-CO₂, 2013), or in the case of sub-fossil mosses, when the samples were growing. [The response \$\Delta^{13}\text{C}\$ to pCO₂ across elevational gradients in modern mosses was then used to calibrate the theoretical model BRYOCARB that has been developed to reconstruct past CO₂ levels based on measurements of \$^{13}\text{C}\$ in paleo bryophytes. Thus, our approach provides two independent estimates of Pliocene CO₂ concentrations – one empirically derived from our transfer function and the other predicted from the BRYOCARB model calibrated to modern mosses and constrained by our paleoclimate reconstructions.](#)

Deleted: vary due

Deleted: to

Deleted: elevation

Deleted: all atmospheric gases, including

Deleted: ,

Deleted: with atmospheric height (h)

Deleted: S

Deleted: atmospheric

Deleted: ($p_i / p_a \rightarrow p_a$), Eq. (2) can be substituted into Eq. (1), such that the natural logarithm of $\Delta^{13}\text{C}_{\text{bryo}}$ varies as a function of the partial pressure of atmospheric CO₂.

Deleted: and time invariant

Deleted: ,

Deleted: , and years in which these samples were collected

Deleted: values

Deleted:

Deleted: →

Formatted: Font: Italic, Subscript

Formatted: Subscript

In order to derive estimates of atmospheric CO₂ concentrations during the Pliocene, isotopic composition of source CO₂ from the atmosphere (ie. $\delta^{13}C_{atm}$) was estimated during the Pliocene to solve for $\Delta^{13}C$ of mosses (Eq.(3)). This was accomplished by simultaneous measurements of $\delta^{13}C$ in the C₃ plant buckbean (*Menyanthes trifoliata* L.) that was identified as a subfossil specimen at the BP site and was also collected from four different sites in the Canadian Boreal Forest. Although it has been demonstrated that $\Delta^{13}C$ of C₃ plant material is sensitive to many factors, including mean annual precipitation and altitude (Diefendorf et al. 2010), there is less variability within biomes, so modern buckbean was sampled from within the Canadian Boreal biome that we suspect is very similar to the BP site based upon paleovegetation (Ballantyne et al. 2010, Fletcher et al. 2017). Measurements of $\delta^{13}C$ on modern buckbean were used to constrain estimates of p_i / p_a using modern estimates of $\delta^{13}C_{atm}$ from when the buckbeans were collected. This constrained modern value of p_i / p_a was then applied to our sub-fossil buckbean samples to estimate $\delta^{13}C_{atm}$ during the Pliocene. All plant and moss material were rinsed and placed in a sonicating bath with deionized water to remove any paleosoil from samples. The diagnostic material for mosses was leafy material, whereas buck bean was identified base on seeds. Therefore, to ensure that our isotopic measurements were made on similar compounds, cellulose was extracted from samples according to Leavitt and Danzer (1993). All carbon isotopic measurements were performed at University of Arizona's environmental isotope laboratory.

Deleted: we first had to estimate the $\delta^{13}C$ of atmospheric CO₂

Deleted: 2

Deleted: cellulose of sub-fossil

Deleted: was also found at the BP site. We also measured $\delta^{13}C$ of modern buckbean to constrain our estimates of p_i / p_a . For constraining our reconstructions of Pliocene CO₂, carbon isotopic measurements were made on sub-fossil mosses (*Scoropodium scorpioides* (Hedw.) Limpr.). All plant and moss material were rinsed in deionized water, and dried prior to cellulose extraction

2.4 Paleotemperature Reconstruction

Paleotemperature estimates were determined based on the distribution of fossilized, sedimentary membrane lipids known as branched glycerol dialkyl glycerol tetraethers (brGDGTs) that are well preserved in peat bogs, soils, and lakes (Powers et al., 2004; Weijers et al., 2007c). These unique lipids are thought to be synthesized by a wide array of Acidobacteria within the soil (Sinninghe Damsté et al., 2011; Sinninghe Damsté et al., 2014) and presumably other bacteria (Sinninghe Damsté et al., 2018) in soils and peat bogs but also in aquatic systems. Previously, it has been established that the degree of methyl branching (expressed in the methylation index of branched tetraethers; MBT) is correlated with mean annual air temperature (MAT), and the relative amount of cyclopentane moieties (expressed in the cyclization index of branched tetraethers; CBT) has been shown to correlate with both soil pH and mean annual air temperature (Weijers et al., 2007b). Because of the relationship of the distribution of these fossilized membrane lipids with these environmental parameters, it has been used for paleoclimate applications in different environments including coastal marine sediments (Bendle et al., 2010; Weijers et al., 2007a), peats (Ballantyne et al., 2010; Naafs et al., 2017), paleosoils (Peterse et al., 2011; Zech et al., 2012), and lacustrine sediments (Loomis et al., 2012; Niemann et al., 2012; Pearson et al., 2011; Zink et al., 2010).

Deleted: ; Sinninghe Damsté et al., 2011

Deleted: i

Improved separation methods (Hopmans et al., 2016) have recently led to the separation and quantification of the 5- and 6-methyl brGDGT isomers that used to be treated as one since the 6-methyl isomers were co-eluting with the 5-methyl isomers (De Jonge et al., 2013). This has led to the definition of new indices and improved MAT calibrations based on the global soil (De Jonge et al., 2014), peat (Naafs et al., 2017), and African lake (Russell et al., 2018) datasets.

Sediment samples were freeze-dried and then ground and homogenized with a mortar and pestle. Next, using the Dionex™ accelerated solvent extraction (ASE), 0.5–1.0 g of sediment was extracted with the solvent mixture of

dichloromethane (DCM):methanol (9:1, v/v) at a temperature of 100°C and a pressure of 1500 psi (5 min each) with 60% flush and purge 60 s. The Caliper Turbovap®LV was utilized to concentrate the collected extract, which was then transferred using DCM and dried over anhydrous Na₂SO₄ before being concentrated again under a gentle stream of N₂ gas. To quantify the amount of GDGTs, 1 µg of an internal standard (C46 GDGT; Huguet et al., 2006) was added to the total lipid extract. Then, the total lipid extract was separated into three fractions using hexane:DCM (9:1, v:v) for the apolar fraction, hexane:DCM (1:1, v:v) for the ketone fraction and DCM:MeOH (1:1, v:v) for the polar fraction, using a column composed of Al₂O₃, which was activated for 2 h at 150°C. The polar fraction, which contained the GDGTs, was dried under a steady stream of N₂ gas and weighed before being then re-dissolved in hexane:isopropanol (99:1, v:v) at a concentration of 10 mg ml⁻¹ and subsequently passed through a 0.45 µm PTFE filter. Finally, the polar fractions were analyzed for GDGTs by ultra-high performance liquid chromatography – atmospheric pressure positive ion chemical ionization – mass spectrometry (UHPLC-APCI-MS) using the method described by Hopmans et al., (2016). The polar fractions of some samples were re-run on the UHPLC-APCI-MS multiple times and the average fractional abundances of the brGDGTs was determined.

For the calculation of brGDGT-based proxies, the brGDGTs are specified by the Roman numerals as indicated in Fig. S1. The 6-methyl brGDGTs are distinguished from the 5-methyl brGDGTs by a prime. The novel indices, including MBT'_{5Me} based on just the 5-methyl brGDGTs and the CBT' that was used to calculate the pH (De Jonge et al., 2014):

$$MBT'_{5Me} = ([Ia] + [Ib] + [Ic]) / ([Ia] + [Ib] + [Ic] + [IIa] + [IIb] + [IIc] + [IIIa] + [IIIb] + [IIIc]) \quad (4)$$

$$CBT' = -^{10}\log\left(\frac{[Ic] + [IIa'] + [IIb'] + [IIc'] + [IIIa'] + [IIIb'] + [IIIc']}{[Ia] + [IIa] + [IIIa]}\right) \quad (5)$$

The square brackets denote the fractional abundance of the brGDGT within the bracket relative to the total brGDGTs. Mean summer air temperature (MST) was determined using the distributions of aquatically produced brGDGTs in the lake calibration developed by Pearson et al. (2011). When this calibration is used the fractional abundances of IIa and IIa' must be summed because these two isomers co-eluted under the chromatographic conditions used by Pearson et al. (2011):

$$MST (^{\circ}C) = 20.9 + 98.1 \times [Ib] - 12 \times ([IIa] + [IIa']) - 20.5 \times [IIIa] \quad (6)$$

MAT and surface water pH were also calculated using a novel calibration created using sediments from East African lakes analysed with the novel chromatography method and based upon MBT'_{5Me} (Russell et al., 2018).

$$MAT = -1.2141 + 32.4223 * MBT'_{5Me} \quad (7)$$

$$\text{Surface water pH} = 8.95 + 2.65 * CBT' \quad (8)$$

Deleted: concentrated

Deleted: on a

Deleted: (

Deleted: in those cases

Deleted: were averaged and those values were used in the transfer functions. The overall estimate error of 2.03°C was determined by using the transfer function error (Ter = 2.0°C) and reproducibility error (Tre = 0.32°C), calculated as the average of the standard deviations from the duplicates

Deleted: ¶

Deleted: The square brackets denote the fractional abundance of the brGDGT within the bracket relative to the total brGDGTs. ¶
Mean annual air temperature (

Deleted:)

Deleted: A

2.5 Vegetation and Fire Reconstruction

For charcoal, a total of thirty 2 cm³ samples were taken at 5 cm intervals from depths from 300 and 301.45 MASL at the BP site, with an additional 2cm³ sample collected at 301.65 MASL. All samples were deflocculated using sodium hexametaphosphate and passed through 500, 250 and 125 µm nested mesh sieves. The residual sample caught on each sieve was then collected in a gridded petri dish and examined using a stereomicroscope at 20-40X magnification to obtain charcoal concentration (fragments cm⁻³). Charcoal area (mm² cm⁻³) was measured for each sample using specialized imaging software from Scion Corporation. For a detailed description of methods see Brown and Power (2013).

Vegetation was reconstructed using pollen and spores (herein pollen) at selected elevations at an upper and lower elevation, that corresponded with changes in charcoal. Samples were processed using standard approaches (Moore et al., 1991), whereby 1cm³ sediment subsamples were treated with 5% KOH to remove humic acids and break up the samples. Carbonates were dissolved using 10% HCl, whereas silicates and organics were removed by HF and acetolysis treatment, respectively. Pollen slides were made by homogenizing 35 µl of residue, measured using a single-channel pipette, with 15 µl of melted glycerin jelly. Slides were counted using a Leica DM4000 B LED compound microscope at 400–630x magnification. A reference collection and published keys (McAndrews et al., 1973; Moore et al., 1991) aided identification.

In addition to tabulating pollen and charcoal, a list of taxa derived from Beaver Pond was previously compiled in Fletcher et al. (2017). Extant species from this list were selected and their modern observations extracted from the Global Biodiversity Information Facility (GBIF.org, 2017). Observation data was grouped by 5° latitude 5° longitude grids cells, and the shared species count calculated using R (R Core Team, 2016). Modern fire frequency was mapped using the MODIS 6 Active Fire Product. The fire pixel detection count per day, within the same 5° latitude 5° longitude grids cells was counted over the ten years 2006–2015, and standardized by area of the cell. The modern climate maps were generated using data from WorldClim 1.4 (Hijmans et al., 2005). The values for the bioclimatic variables mean temperature of the warmest quarter (equivalent to mean summer air temperature; MST) and precipitation of the warmest quarter (summer precipitation) were also averaged by grid cell. The shared species count, climate values, and fire day detections were mapped to the northern polar stereographic projection in ArcMap 10.1.

3 Results

3.1 Geochronology

The burial dating results with ²⁶Al/¹⁰Be in quartz sand at 10 m below modern depth provides four individual ages. From shallowest to deepest, the burial ages are 3.6 +1.5/-0.5 Ma, 3.9 +3.7/-0.5 Ma, 4.1 +5.8/-0.4 Ma, and 4.0 +1.5/-0.4 Ma (Table S3), with an unweighted mean age of 3.9 Ma. [The convoluted probability distribution function yields a maximum probability age of 4.5 Ma. Unfortunately, the positive tails of the probability distribution functions of two of the samples exceeds the radiodecay saturation limit of the burial age. Therefore, their probability distributions do not reflect the actual age probabilities and uncertainty. Given the positive tail in the probability distribution functions, and the inability to convolve all samples, we recommend using the unweighted mean age, 3.9 Ma, with an uncertainty](#)

Deleted: and

Deleted:

Deleted: T

of +1.5/-0.5 Ma as indicated by the two samples with unsaturated limits. Despite the apparent upward younging of the individual burial ages, the 1 σ -uncertainties overlap rendering the samples indistinguishable.

3.2 Atmospheric CO₂ Reconstruction

As expected, carbon isotopic discrimination in mosses shows a positive relationship with partial pressure of atmospheric CO₂ both in empirical observations and theoretical predictions (Fig. 3). However, a much greater change in $\Delta^{13}\text{C}_{\text{moss}}$ is observed in response to p_a than is predicted from the optimized BRYOCARB simulations. The empirical fit to the observed change in $\Delta^{13}\text{C}_{\text{moss}}$ in response to p_a is slightly better (RMSE = 1.8 ‰) than the theoretical prediction from the BRYOCARB model (RMSE = 2.1 ‰), but the slopes are quite different, with our empirical slope (0.56 ‰/ p_a) an order of magnitude greater than the linear approximation of the BRYOCARB slope (0.07 ‰/ p_a), suggesting that other non-linear processes and not just p_a may be affecting $\delta^{13}\text{C}_{\text{moss}}$ variability with elevation.

While there does appear to be a global relationship between p_a and $\Delta^{13}\text{C}$ of mosses, there are notable differences among sites. Moss $\Delta^{13}\text{C}$ values tended to be generally lower in the Swiss Alps (mean = 17.4 ‰) and higher in Hawaii (mean = 20.6 ‰) and the slope of the relationship between p_a and $\Delta^{13}\text{C}$ appears to vary across sites with the Andes having the smallest slope and Poland having a much greater slope. We used the BRYOCARB model to test the sensitivity of $\Delta^{13}\text{C}$ to other variables that change as a function of elevation (e.g. temperature and $p\text{O}_2$). According to our BRYOCARB simulations, with all other variables held constant decreased temperature with increased elevation should slow metabolic rates resulting in an increase in $\Delta^{13}\text{C}$ (Supplemental Figure S3), which directly contradicts observations (Fig. 3). Furthermore, the range of mean summer temperature estimates from the Pliocene BP site could only explain ~0.2 ‰ isotopic response in our moss samples. Similarly we evaluated the effect of just changing $p\text{O}_2$ in our BRYOCARB simulations and found a decrease in $\Delta^{13}\text{C}$ with increasing $p\text{O}_2$ that is opposite to the $\Delta^{13}\text{C}$ response of mosses to partial pressure across all elevational transects. We also evaluated model performance using a global standard atmospheric sea level pressure of 101.325 kPa, or site-specific atmospheric pressure estimates from ERA-interim reanalysis data. We found that the model using site specific atmospheric pressure estimates performed better at predicting $\Delta^{13}\text{C}_{\text{moss}}$ (RMSE = 1.096 ‰) than the model using global standard atmospheric sea level pressure (RMSE = 1.216 ‰). Therefore, it appears that partial pressure of atmospheric CO₂ is the primary physical mechanism explaining the global relationship between $\Delta^{13}\text{C}$ of mosses and elevation and that other factors, such as water availability that may be mediated by different lapse rates (Ménot and Burns, 2001; Royles et al., 2014; Skrzypek et al., 2007; Waite and Sack, 2011), may explain variability among sites. Thus, the optimal model characterizing the observed modern relationship between $\Delta^{13}\text{C}_{\text{moss}}$ and the p_a was:

$$13\text{C}\Delta^{13}\text{C}_{\text{moss}} = 0.56 \times p\text{CO}_2 + 1.55 \quad (9)$$

Based on our analysis of cellulose extracted from four different *Menyanthes* L. (i.e. buckbean) plants growing at four different locations in the modern boreal forest, we found $\Delta^{13}\text{C}$ of buckbean to be fairly constant 16 ± 0.4 ‰, yielding an estimate of p_i/p_a in modern buckbean of 0.51. Applying this modern of p_i/p_a to our $\delta^{13}\text{C}$ measurements from sub-fossil buckbean we obtained estimates of $\delta^{13}\text{C}_{\text{atm}}$ during the Pliocene of -6.23 ± 0.9 ‰. Using our empirical

Deleted: The convoluted probability distribution function yields a maximum probability age of 4.5 Ma. The optimized ages for the top and bottom sample were 3.6 and 4.0 Ma, in agreement with the individual most probable ages. Optimized ages could not be computed for the two middle samples owing to the large uncertainties in $^{26}\text{Al}/^{27}\text{Al}$ measurement which caused the uncertainties to extend beyond the maximum saturation burial ages (ca. 8 Ma). Despite the apparent upward younging of the burial ages, the 1 σ -uncertainties overlap rendering the samples indistinguishable. Given the asymmetry in the probability distribution functions, and the inability to convolve all samples, the unweighted mean age is 3.9 Ma, with an uncertainty of +1.5/-0.5 Ma as indicated by the two samples with unsaturated limits. The age of the Beaver Pond peat is stratigraphically younger, however considering time for lateral channel migration and aggradation on the contemporaneous braid plain, the peat age is likely older by 104 to 105 years, i.e. within the uncertainty of the mean burial date.

Deleted: (Fig. 3) and, as predicted from theory, the natural logarithm of carbon isotopic discrimination in mosses ($\Delta^{13}\text{C}_{\text{moss}}$) is responsive to p_a . Consistent with the exponential relationship between elevation and atmospheric pressure (Eq. 2) the relationship is non-linear with a greater change in p_a and thus a greater change in $\Delta^{13}\text{C}_{\text{moss}}$ at lower elevations. Despite fitting our model to $\text{Ln}(\Delta^{13}\text{C}_{\text{moss}})$, we found a slightly better fit based on a second order polynomial

Deleted: 1

Deleted: 096

Deleted: a linear model

Deleted: 1.097

Formatted: Subscript

Deleted: While these subtle differences are probably due to local climate affects, it appears that p_a is the primary physical mechanism explaining the previously reported global relationship between $\Delta^{13}\text{C}$ of mosses and elevation globally across all sites (Ménot and Burns, 2001; Royles et al., 2014; Skrzypek et al., 2007; Waite and Sack, 2011).

Deleted: the second order polynomial

Deleted: This polynomial was solved numerically to derive estimates of $p\text{CO}_2$ during the Pliocene based on sub-fossil moss samples collected at the BP site.

transfer function (Eq. 9) in combination with these estimates of $\delta^{13}\text{C}_{\text{atm}}$, we were able to approximate atmospheric CO_2 concentrations over the Pliocene interval captured at the BP site (Fig. 4). We estimated a mean atmospheric CO_2 concentration over this interval of 410 ± 50 ppm (mean \pm transfer error and instrument error) with considerable variability between a minimum atmospheric CO_2 concentration of 296 ppm and a maximum atmospheric CO_2 concentration of 480 ppm. Predicted values of Pliocene CO_2 from the BRYOCARB model were slightly higher at 510 ppm, but the single standard deviation across all estimates was extremely high (967 ppm), suggesting that the BRYOCARB simulations are not significantly different from our empirical model estimates; however, the BRYOCARB model is too sensitive to our range of $\Delta^{13}\text{C}_{\text{moss}}$ estimates and thus not very precise.

Deleted: allowed us

Deleted: 4

Deleted: 70

Deleted: 7

3.3 Paleotemperature Estimates

Deleted: Overall, this proxy approach had a prediction uncertainty of less than 10% of the estimate ($1\sigma = 35$ ppm).

3.3.1 Provenance of branched GDGTs

Previously, brGDGT derived MAT estimates (-0.6 ± 5.0 °C) from BP sediments were developed using the older chromatography methods that did not separate the 5- and 6- methyl brGDGTs, and a soil calibration (Ballantyne et al., 2010). In marine and lacustrine sediments, bacterial brGDGTs were thought to originate predominantly from continental soil erosion arriving in the sediments through terrestrial runoff, however, a number of more recent studies have indicated aquatically produced brGDGTs could be affecting the distribution of the sedimentary brGDGTs and thus the temperature estimates based upon them (Warden et al., 2016; Zell et al., 2013; Zhu et al., 2011). Since the discovery that sedimentary brGDGTs can have varying sources, different calibrations have been developed depending on the origin of the brGDGTs, i.e. soil calibration (De Jonge et al., 2014), peat calibration (Naafs et al., 2017) and aquatic calibrations (i.e. Foster et al., 2016; Pearson et al., 2011; Russell et al., 2018). Therefore, several studies have recommended that the potential sources of the sedimentary brGDGTs should be investigated before attempting to use brGDGTs for paleoclimate applications (De Jonge et al., 2015; Warden et al., 2016; Yang et al., 2013; Zell et al., 2013). In this study, we examine the distribution of brGDGTs in an attempt to determine their origin and consequently the most appropriate calibration to utilize in order to reconstruct temperatures from the BP sediments.

Branched GDGTs IIIa and IIIa' on average had the highest fractional abundance of the brGDGTs detected in the BP sediments (see Fig. S1 for structures; Table S1). A previous study established that when plotted in a ternary diagram the fractional abundances of the tetra-, penta- and hexamethylated brGDGTs, soils lie within a distinct area (Sinninghe Damsté, 2016). To assess whether the brGDGTs in the BP deposit were predominantly derived from soils, we compared the fractional abundances of the tetra-, penta- and hexamethylated brGDGTs in the BP sediments to those from modern datasets in a ternary diagram (Fig. 6). Since the contribution of brGDGTs from either peat or aquatic production could affect the use of brGDGTs for paleoclimate application, in addition to comparing the samples to the global soil dataset (De Jonge et al., 2014), peat and lacustrine sediment samples were added into the ternary plot to help elucidate the provenance of brGDGTs in the BP sediments. According to Sinninghe Damsté (2016), it is imperative to only compare samples in a ternary diagram like this where all of the datasets were analyzed with the novel methods that separate the 5- and 6-methyl brGDGTs since the improved separation can result in an increased abundance of hexamethylated brGDGTs. Recently, samples from East African lake sediments were analyzed using these new methods (Russell et al., 2018) and so these samples were included in the ternary plot for comparison (Fig.

6). Although the lakes from the East African dataset are all from a tropical area, they vary widely in altitude and, thus, in MAT. We separated them into three categories by MAT (lakes >20°C, lakes between 10-20°C and lakes <10°C). By comparing all the samples in the ternary plot, it was evident that the BP samples plotted closest to the lacustrine sediment samples from regions in East Africa with a MAT <10°C, suggesting that the provenance of the majority of the brGDGTs from the BP sediments was not soil or peat but lacustrine aquatic production.

The average estimated surface water pH for the BP sediments (8.6 ± 0.2) calculated using eq. (8), is within the 6–9 range typical of lakes and rivers (Mattson, 1999). This value is near the upper limit of rich fens characterized by the presence of *S. scorpioides* (Kooijman and Westhoff, 1995; Kooijman and Paulissen, 2006) and is higher than what would be expected for peat-bog sediments that are acidic (pH 3–6; Clymo, 1964) and which constitute most of the peats studied by Naafs et al. (2017). A predominant origin from lake aquatic production is in keeping with previous interpretation of the paleoenvironment of the BP site, which was at least at times covered by water as evidenced by fresh water diatoms, fish remains and gnawed beaver sticks in the sediment (Mitchell et al., 2016).

3.3.2 Aquatic Temperature Transfer Function

Since there is evidence that the majority of the brGDGTs in the BP sediments are aquatically produced, an aquatic transfer function was used for reconstructing temperature. When we apply the African lake calibration (Eq. 7), the resulting estimated MAT for BP is 7.1 ± 1.0 °C. This value is high compared to other previously published estimates from varying proxies, which have estimated MAT in this region to be in the range of -5.5 to 0.8°C, (Ballantyne et al., 2010; Ballantyne et al., 2006; Csank et al., 2011a; Csank et al., 2011b; Fletcher et al., 2017). A concern when applying this calibration is that it is based on lakes from an equatorial region that does not experience substantial seasonality, whereas, the Pliocene Arctic BP site did experience substantial seasonality (Fletcher et al., 2017). Biological production (including brGDGT production) in BP was likely skewed towards summer and, therefore, summer temperature has a larger influence on the reconstructed MAT. Unfortunately, no global lake calibration set using individually quantified 5- and 6-methyl brGDGTs is yet available. Therefore, to calculate mean summer air temperatures (MST, Eq. 6) we applied the aquatic transfer function developed by Pearson et al. (2011) by combining the individual fractional abundances of the 5- and 6-methyl brGDGTs. The Pearson et al. (2011) calibration was based on a global suite of lake sediments including samples from the Arctic, thus covering a greater range of seasonal variability. The resulting average estimated mean summer temperature was 15.4 ± 0.8 °C, with temperatures ranging between 14.1 and 17.4 °C (Fig. 4). This is in good agreement with recent estimates based on Climate Reconstruction Analysis using Coexistence Likelihood Estimation (CRACLE; Fletcher et al., 2017) that concluded that MSTs at BP during the Pliocene were approximately 13 to 15°C.

3.4 Vegetation and Fire Reconstruction

All sediment samples from BP contained charcoal (Fig. 4), indicating the consistent prevalence of biomass burning in the High Arctic during this time period. However, counts were variable throughout the section, with the middle and lower sections (18 fragments cm⁻³) containing less charcoal compared to the upper section upper section (710 fragments cm⁻³). Overall, samples from BP contained on average 100.0 ± 165 fragments cm⁻³ (mean ± 1 σ), with

charcoal area averaging $12.3 \pm 20.2 \text{ mm}^2 \text{ cm}^{-3}$. The variability of charcoal within any given sample was relatively low with a 1σ among charcoal area of approximately $2 \text{ mm}^2 \text{ cm}^{-3}$.

The three sections analysed for pollen reveal variations in vegetation (Figs. 4 and 5). Near the bottom of the section (300.3-300.4 MASL), *Larix* (26%) and *Betula* (17%) were the dominant trees. *Alnus* (6%) and *Salix* (6%) together with ericaceous pollen (4%) were relatively high. In contrast, low numbers of *Picea* (3%), *Pinus* (3%) and fern spores were recorded. Additional wetland taxa like *Myrica* (5%) and Cyperaceae (6%) were also noted. Overall, the non-arboreal (23%) signal was well developed. Crumpled and/or ruptured inaperturate grains with surface sculpturing that varied from scabrate to verrucate were noted in the assemblage (12%), but could not be definitely identified. It is possible that these grains represent *Populus*, Cupressaceae or additional Cyperaceae pollen. Between 301.15-301.25 MASL, *Larix* (38%) and *Betula* (21%) increased in abundance, followed by ferns (7%). Cyperaceae remained at similar levels (6%) whereas *Picea* and *Pinus* decreased to 2% and 1%, respectively. Unidentified inaperturate types collectively averaged 14%. *Larix* pollen (23%) remained abundant near the top of the section (301.35-301.45 MASL), whereas *Betula* (2%) decreased. *Picea* (16%) *Pinus* (6%) and ferns (23%) increased in abundance. Of the ferns, trilete spores and cf. *Botrychium* were most abundant, followed by cf. *Dryopteris*. Inaperturate unknowns (10%) were also observed. Other notables included Ericaceae (2%) and Cyperaceae (2%). While rare, Onagraceae grains were also observed (Fig. 5).

According to GBIF-based mapping exercise, the paleofloral assemblage at BP most closely resembles modern day vegetation found in northern North America, particularly on the eastern margin (e.g. New Hampshire, New Brunswick and Nova Scotia) and the western margin (Alaska, Washington, British Columbia, and Alberta; Fig. 7a), and central Fennoscandia. Of these areas, the western coast of northern North America and eastern coast of southern Sweden has the most similarity to the reconstructed BP climate in terms of MST (Fig. 7b) and summer precipitation (Fig. 7c).

While high counts of active fire days are common in the western part of the North American boreal forest, it is not as common in the eastern part of the North American boreal forest (Fig. 7d), likely due to the differences in the precipitation regime. There was also low fire counts in Fennoscandia likely due to historical severe fire suppression (Brown and Giesecke, 2014; Niklasson and Granström, 2004). Therefore, based on our reconstruction of the climate and ecology of the BP site, our results suggest that BP most closely resembled a boreal-type forest ecosystem shaped by fire, similar to those of Washington, British Columbia, Northwest Territories, Yukon and Alaska (but see Sect. 4.3).

4 DISCUSSION

4.1 Geochronology

The plant and animal fossil assemblages observed at BP suggest a depositional age between 3 and 5 Ma (Matthews Jr and Oviden, 1990; Tedford and Harington, 2003). This biostratigraphic age was corroborated with an amino-acid racemization age ($>2.4 \pm 0.5 \text{ Ma}$) and Sr-correlation age (2.8–5.1 Ma) on shells (Brigham-Grette and Carter, 1992) in biostratigraphically correlated sediments on Meighen Island, situated 375 km to the west-north-west. The previously calculated burial age of 3.4 Ma for the BP site is a minimum age because no post-depositional production of ^{26}Al or

^{10}Be by muons was assumed. If the samples are considered to have been buried at only the current depth (ca. 10 m, see supplemental data) then the ages plot to the left and outside of the burial field, indicating that the burial depth was significantly deeper for most of the post-depositional history. The revised cosmogenic nuclide burial age is $3.9 \pm 1.5/-0.5$ Ma. It is the best interpretation of burial age data based on improved production rate systematics (e.g. Lifton et al., 2014), and more reasonable estimates of erosion rate and ice cover since the mid-Pliocene (see Table S4). As the stratigraphic position of the cosmogenic samples is very close to the BP peat layers, we interpret the age to represent the approximate time that the peat was deposited.

4.2 Pliocene atmospheric CO_2 levels

We have derived a transfer function that allows us to predict the partial pressure of atmospheric CO_2 in Earths' past based on carbon isotopic measurements in bryophytes. However, many of the studies included in our transfer function identify other mechanisms that may also influence carbon isotopic discrimination in bryophytes. Because these other mechanisms may violate the assumptions of applying this transfer function to the past or contribute error to our reconstructions of atmospheric CO_2 concentrations during the Pliocene, we discuss these mechanisms below.

It has been suggested that in the absence of stomatal regulation, that surface water may control the gradient in partial pressure (i.e. p_i/p_a) in bryophytes (White et al., 1994), due to the greater resistance to diffusion of CO_2 in water than in the atmosphere. For instance, Ménot and Burns (2001) found that most mosses growing along an elevational transect in Switzerland experienced discrimination with elevation in response to decreased partial pressure, except one species *Sphagnum cuspidatum* Ehrh. ex Hoffm., which grows almost exclusively in wet hollows. In a study of Hawaiian bryophytes Waite and Sack (2011) found consistent slopes of less isotopic discrimination with elevation in all species, however, species growing on young substrate showed significantly less isotopic discrimination. The most likely explanation is that lack of canopy cover on the older substrates lead to greater photosynthetic rates, which lead to reduced p_i . Lastly, decreased discrimination of mosses growing along an elevational transect in Poland (Skrzypek et al., 2007), was found to be highly correlated with temperature. Although temperature is the primary factor driving most metabolic reactions, it does not provide a physical mechanism explaining the relationship between elevation and isotopic discrimination in mosses. Skrzypek et al. (2007) found slightly different relationships between elevation and carbon isotopic discrimination in mosses growing on the windward versus leeward side of their elevational transects suggesting that changes in lapse rate may also play a factor. Collectively, these studies suggest that microclimatic factors may explain differences in isotopic discrimination of mosses within and among different sites possibly contributing to different intercepts for sites reported in Fig. 3, and that dry vs. moist lapse rates may also play a role in regulating the different slopes among sites. In fact, the greatest elevational range reported among sites was for the elevational transect in the Andes (320 to 3100 m), but this site did not experience the widest range in $\Delta^{13}\text{C}_{\text{moss}}$. This tropical transect had a very moist lapse rate resulting in the least change in atmospheric temperature and humidity with elevation. Nonetheless, by projecting these data as a function of partial pressure we provide a physical mechanism to explain variations in moss carbon isotopic values globally and we help reconcile the previously reported empirical relationships, such as elevation, temperature, and over-story, all of which tend to be covariates of decreasing partial pressure with elevation. While differences in microclimate and lapse rate are clearly important factors in regulating

$\Delta^{13}\text{C}_{\text{moss}}$, these factors contribute to the global error in our model for predicting p_a and ultimately to uncertainties in our estimates of atmospheric CO_2 concentrations during the Pliocene.

Our reconstructions of CO_2 concentration for this mid-Pliocene interval are within the range of previously reported CO_2 estimates, tending to agree with alkenone estimates from Pagani et al. (2010). This suggests that CO_2 concentrations during this warm Pliocene interval were above 400 ppm. In fact our mean Pliocene value (410 ± 50 ppm) is not statistically different from the alkenone based estimates (357 ± 47 ppm) previously reported by Pagani et al. (2010) and our theoretical predictions based on BRYOCARB calibrated to modern $\Delta^{13}\text{C}_{\text{moss}}$ values indicate CO_2 concentrations of approximately 510 ppm, albeit highly variable due to the sensitivity of the model simulations. Generally, our estimates showed sustained atmospheric CO_2 estimates of slightly higher than 400 ppm with only two anomalously low values (Fig. 4). These estimates could represent an actual reduction in atmospheric CO_2 , or they might be artefacts of sampling or analysis. It should be noted that poor preservation and a possible shift in dominant moss species to *Drepanocladus* spp. was evident in samples corresponding to these two anomalously low CO_2 estimates. While one of these samples contained only 0.17 mg/C and a $\delta^{13}\text{C}$ value of -20.9 ‰, the other contained 0.88 mg/C and a $\delta^{13}\text{C}$ value of -25.0 ‰. Thus, it is conceivable that the sample corresponding to the atmospheric CO_2 estimate of 335 ppm, might be approaching our minimum detection limit and should be verified in subsequent studies.

It should also be noted that changes in growth rate due to phosphorus availability and biases in shell size are known to contribute uncertainty to alkenone-derived CO_2 concentration estimates (Seki et al., 2010). Similar assumptions may affect boron-derived estimates of CO_2 concentrations. For instance, a recent update on the global boron cycle estimates the mean residence time of boron to be ~ 1.5 Ma and suggests that boron isotopes may not be sensitive to ocean pH on timescales less than 1 Ma (Schlesinger and Vengosh, 2016). This may help explain the apparent lack of variability in boron isotope based CO_2 estimates during the Pliocene (Hönisch et al., 2009; Tripathi et al., 2009); however, boron isotopes do seem to reproduce the CO_2 variability measured in ice cores over the Pleistocene (Hönisch et al., 2009). Overall, our estimates using two independent approaches suggest that Pliocene CO_2 concentrations during this interval ranged between 400 and 500 ppm are consistent with recent estimates derived from both alkenones and from boron isotopes (Martinez-Boti et al., 2015; Seki et al., 2010).

There are numerous assumptions based on known uncertainties in our CO_2 reconstruction approach. First of all, our empirically based approach requires some estimate of the isotopic ratio of atmospheric CO_2 during this time, which we derive from C3 vegetation (Fletcher et al., 2008; White et al., 1994). Here we estimate the isotopic composition of the atmosphere over the Pliocene to be $\delta^{13}\text{C} = -6.23 \pm 0.9$ ‰, which is within the range of values recorded over glacial-interglacial intervals in ice cores $\delta^{13}\text{C} = -6.2$ to -7.0 ‰ (Bauska et al., 2016) and consistent with estimates derived from carbon isotope measurements of foraminifera (Ravelo et al., 2004). If we assume that the isotopic composition of atmospheric CO_2 was -8.2 ‰ during the Pliocene and similar to today due to greater transfer of lighter carbon from the terrestrial reservoir to the atmospheric reservoir, that would result in reduced $\Delta^{13}\text{C}_{\text{moss}}$ and decreases in our mean estimate of atmospheric CO_2 to approximately 390 ppm. This adjustment to our original estimate of $\delta^{13}\text{C}$ of atmospheric CO_2 would bring our atmospheric CO_2 estimate more in line with previous reconstructions, but is still within the range of error of our original estimate.

Deleted: 4

Deleted: approximately

Deleted: 5

Deleted: four

Deleted: 270

Deleted: Overall, these CO_2 estimates are consistent with recent estimates derived from both alkenones and from boron isotopes (Martinez-Boti et al., 2015; Seki et al., 2010).

Deleted: and boron/calcium

Deleted: Our atmospheric CO_2 estimates are in the range of previous estimates, although the values seem slightly high and are variable, suggesting that these estimates probably represent atmospheric conditions during a Pliocene warm interval and not necessarily an integrated average over the entire Pliocene.

Deleted: 42

Formatted: Superscript

Another critical assumption of our approach is that the total pressure of the atmosphere has not changed at the BP site since the Pliocene either through increased partial pressure of constituent gases or more likely through changes in elevation due to dynamic isostasy. The current elevation of the site is approximately 380 MASL with a summertime total atmospheric pressure of approximate 88.5 kPa. If we assume that the site was at 0 m during the Pliocene that would increase the total summertime atmospheric pressure to 93.9 kPa and would decrease our Pliocene CO₂ estimates to about 390 ppm. However, estimates of dynamic eustasy since the Pliocene from paleoshorelines at lower latitudes are between 5 and 20 m (Rovere et al., 2014), suggesting that our assumptions regarding elevation at the site probably have a negligible impact on our estimates of Pliocene atmospheric CO₂ concentrations, especially given the uncertainty of the proxy approach. Therefore, the assumptions to our approach in estimating past CO₂ may be leading to estimates that are biased slightly high relative to previous estimates. When these assumptions are considered, our estimates still suggest atmospheric CO₂ concentrations around 400 ppm or above during this Pliocene warm interval.

4.3 Fire, vegetation, climate

Wildfire is a key driver of ecological processes in modern boreal forests (Flannigan et al., 2009; Ryan, 2002), and although historically rare, is becoming more frequent in the tundra in recent years (Mack et al., 2011). The modern increase in fire frequency is likely as a consequence of atmospheric CO₂ driven climate warming and feedbacks such as reduced sea ice extent (Hu et al., 2010), because the probability of fire is highest where temperature and moisture are conducive to growth and drying of fuels followed by conditions that favor ignition (Whitman et al., 2015). Young et al. (2017) confirmed the importance of summer warmth and moisture availability patterns in predicting fire across Alaska, highlighting a July temperature of ~13.5 °C as a key threshold for fire across Alaska.

The abundance of charcoal at BP demonstrates that climatic conditions were conducive for ignition and that sufficient biomass available for combustion existed across the landscape. brGDGTs derived temperature estimates suggest mean summer temperatures at BP exceeded the ~13.5 °C threshold (Young et al., 2017) that drastically increases the chance of wildfire. An increase in atmospheric convection has been simulated in response to diminished sea-ice during warmer intervals (Abbot and Tziperman, 2008), but this study did not confirm if this increase in atmospheric convection was sufficient to cause lightning ignitions. An alternative ignition source for combustion of biomass on Ellesmere Island during the Pliocene is coal seam fires, which have been documented to be burning at this time (Estrada et al., 2009). However, given the interaction of summer warmth and ignition by lightning within the same climate range as posited for BP, we consider lightning the most likely source of ignition for Pliocene fires in the High Arctic.

Fire return intervals cannot be calculated from the BP charcoal counts due to the absence of a satisfactory age-depth model and discontinuous sampling. As strong interactions are observed between fire regime and ecosystem assemblage in the boreal forest (Brown and Giesecke, 2014; Kasischke and Turetsky, 2006), and in response to climate, comparison with modern fire regimes for areas with shared species compositions and climates may inform a potential range of mean fire return interval (MFRI).

Matthews and Fyles (2000) indicated that the Pliocene BP environment was characterized by an open larch dominated forest-tundra environment, sharing most species in common with those now found in three regions,

Deleted: 42

Formatted: Not Highlight

Deleted: exceeding

Formatted: Not Highlight

Formatted: Not Highlight

including central Alaska to Washington in western North America, the region centered around the Canadian/US border in eastern North America, as well as Fennoscandia in Europe. The modern area with the most species in common with BP is central northern Alaska (Fig. 7A). The area over which shared species were calculated is largely tundra, but includes the ecotone between tundra and boreal forest. Other zones that share many species with BP are continuous with Alaska down the western coast of North America to the region around the border of Canada and the United States, the eastern coast of North America in the region around the border of Canada and the United States (~50°N), and central Fennoscandia. Of these zones, the MST of Alaskan tundra sites (6–9°C) are less similar to BP (15.4°C) than ~50°N on both western and eastern coastal North American sites and central Fennoscandia (12–18°C, Fig. 7B). The eastern coast of North America has higher rainfall during the summer (>270 mm), than the west coast and Alaska (Fig. 7C), which correlates to the timing of western fires. The low summer precipitation for much of the west (<200 mm), is consistent with previously published summer precipitation estimates for BP (~190 mm). As a result, the fire regime of the west coast ~50°N may be a better analogue for BP than the east coast of North America. In central Fennoscandia there is also a west vs. east coastal variation in summer precipitation with the western, Nordic part of the region experiencing higher summer precipitation (252–>288 mm), than the more similar eastern, Swedish part of the region (~198 mm).

Comparison to modern fire detection data (Fig. 7D) suggests that the two regions most climatically similar to BP, ~50°N western North America and central Sweden, have radically different fire regimes. This is likely caused by historical fire suppression in Sweden that limits utility of very modern data for comparison in this study (Brown and Giesecke, 2014; Niklasson and Granström, 2004). To understand the fire regimes as shaped by climate and species composition rather than human impacts, we considered both the modern and recent Holocene reconstructions for these regions (Table 1). This shows that, a) within any region variation arises from the complex spatial patterning of fire across landscapes, and b) that the regions most similar to BP (~50°N western North American and eastern Fennoscandian reconstructions for the recent Holocene) have shorter fire return intervals than the cooler Alaskan tundra or wetter summer ~50°N eastern North American coast.

While the shared species for Siberia appears low, the number of observations in the modern biodiversity database used is likewise low – perhaps causatively so. Given the similar climate to BP on the Central Siberian Plateau and some key aspects of the floras in Siberia such as the dominance of larch, we considered the fire regime of the larch forests of Siberia. Kharuk et al. (2016; 2011) studied MFRI across Siberia, from 64°N to 71°N, the northern limit of larch stands. They found an average MFRI across that range of 110 years, with MFRI increasing from 80 years in the southern latitudes to ~300 in the north (Table 1). Based on similarity of the climate variables, the more southerly MFRI (~80 years) may be a better analogue. Key differences between boreal fires in the North America compared to Russia are a higher fire frequency with more burned area in Russia, but a much lower crown fire and a difference in timing of disturbance, with spring fires prevailing in Russia compared to mid-summer fires in western Canada (de Groot et al., 2013; Rogers et al., 2015).

The pollen-based vegetation reconstruction derived in this study indicates that open *Larix-Betula* parkland persisted in the basal (300.3–300.4 MASL) parts of the sequence. Groundcover was additionally dominated by shrub birch, ericaceous heath and ferns. While the regional climate may have been somewhat dry, the record suggests that, locally,

a moist fen environment dominated by Cyperaceae, existed near the sampling location. Shrubs including *Alnus* and *Salix* likely occupied the wetland margins.

The corresponding relatively low concentration of charcoal may reflect lower severity fires or higher sedimentation rates. If the former, it is posited that a surface fire regime existed. This premise is supported by the fire ecology characteristics of the dominant vegetation. *Larix* does not support crown fires due to leaf moisture content (de Groot et al., 2013) and self-pruning (Kobayashi et al., 2007). The persistence and success of larch in modern-day Siberia appears to be driven by its high growth rate (Jacquelyn et al., 2017) tolerance of frequent surface fire due to thick lower bark (Kobayashi et al., 2007) and tolerance of spring drought due to its deciduous habit (Berg and Chapin III, 1994). Arboreal *Betula* are very intolerant of fire and easily girdled. However, they are quick to resprout and are often found in areas with short fire return intervals. Like *Larix*, arboreal *Betula* have high moisture content of their foliage and are not prone to crown fires. *Betula nana* L., an extant dwarf birch, is a fire endurer that resprouts from underground rhizomes or roots (Racine et al., 1987) thus regenerating quickly following lower severity fires (de Groot et al., 1997). The vegetation and fire regime characteristics are similar further up the sequence at 301.15-301.25 MASL, with the exception that ferns increased in abundance while heath decreased.

In the upper part of the sequence (301.35-301.45 MASL), where charcoal was abundant, the *Larix-Betula* parkland was replaced by a mixed boreal forest assemblage with a fern understory. Canopy cover was more closed compared to the preceding intervals. The forest was dominated by *Larix* and *Picea*, with lesser amounts of *Pinus*. While *Betula* remained part of the forest, it decreased in abundance possibly due to increased competition with the conifers. Based on exploratory CRACLE analyses of climate preferences using GBIF occurrence data (GBIF.org, 2018a, b, c, d) of the dominant taxa (*Larix-Betula* vs. *Larix-Picea-Pinus*), the expansion of conifers could indicate slightly warmer summers (MST ~15.8 °C vs. 17.1 °C). This result differs from the stable MST estimated by bacterial tetrathers, although within reported error, and the small change is certainly within the climate distributions of both communities. The analyses also suggest that slightly drier conditions may have prevailed during the three wettest months (249-285mm vs. 192-219mm). While the interaction between climate, vegetation and fire is complex, small changes in MST and precipitation could have directly altered both the vegetation and fire regime, which in turn further promoted fire adapted taxa. In addition to regional climatic factors, community change at the site may have been further influenced by local hydrological conditions, such as channel migration, pond infilling and ecosystem engineering by beaver (*Cantor spp.*).

The high charcoal content suggests that fire was an important disturbance mechanism, although it could also reflect a slow sedimentation rate. If the former, it is likely that frequent, mixed severity fires persisted. While *Larix* is associated with surface fire, *Picea* and *Pinus* are adapted to higher intensity crown fires. A crown fire regime may have established as conifers expanded, altering fuel loads and flammability. For example, black spruce sheds highly flammable needles, its lower branches can act as fuel ladders facilitating crown fires (Kasischke et al., 2008), and it was previously tentatively identified at BP (Fletcher et al., 2017). While it has thin bark and shallow roots maladapted to survive fire (Auclair, 1985; Brown, 2008; Kasischke et al., 2008), it releases large numbers of seeds from semi-serotinous cones, leading to rapid re-establishment (Côté et al., 2003). The documentation of Onagraceae pollen at the

Deleted: .

Deleted: is in contrast to

Deleted: s

Deleted: the aforementioned changes in

Deleted: climate

Deleted: and

top of the sequence could potentially reflect post-fire succession. For example, the species *Epilobium angustifolium* L. is an early-seral colonizer of disturbed (i.e. burnt) sites, pollinated by insects.

It is possible that the *Larix-Betula* parkland dominated intervals correspond to the peat- and sand-stratigraphic Units II and III described by Mitchell et al. (2016), whereas the mixed boreal forest in the upper part of the sequence is contemporaneous with Unit IV, described as peat and peaty sand, coarsening upwards. While it is clear that the vegetation and fire regimes changed through time at this Arctic site, CO₂ and temperatures appear more stable, or at least to have no apparent trend. Thus, it is suggested that the fire regime at BP was primarily regulated by regional climate and vegetation, and perhaps additionally by changing local hydrological conditions. Regarding climate, MST remained high enough ($\geq \sim 13.5^{\circ}\text{C}$) throughout the sequence to allow for fire disturbance and the pollen suggests that temperatures may have marginally increased in the upper part of the sequence. Alternatively, other climate variables, such as the precipitation regime, or local hydrological change may have initiated the change in community. Up-sequence changes in vegetation undoubtedly influenced fine fuel loads and flammability. Indeed, the fire ecological characteristics of the vegetation are consistent with a regional surface fire regime yielding to a crown fire regime.

Betula and *Alnus*, which occurred earlier in the depositional sequence, are favored by beaver in foraging (Busher, 1996; Haarberg and Rosell, 2006; Jenkins, 1979). Moreover, the presence of sticks cut by beaver in Unit III reveals that beavers were indeed at the site, moistening the local land surface. The lack of beaver cut sticks and changes in sediment in Unit IV may indicate that the beavers abandoned the site, possibly in response to changes in vegetation (i.e. increased conifers and decreased *Betula*) limiting preferred forage or due to lateral channel migration, as evidenced by the coarsening upward sequence described by Mitchell et al. (2016). As a result, the local land surface may have become somewhat drier, contemporaneous with the change towards *Larix-Picea-Pinus* forest and a mixed severity fire regime.

Critically, the charcoal record suggests that there was substantial biomass burning that could have been a feedback mechanism amplifying or dampening warming during the Pliocene due to its prevalence through time, and the complex direct impacts on the surface radiative budget and direct and indirect effects on the top of the atmosphere radiative budget (Feng et al., 2016). Further investigation is warranted to better characterize the fire regime to improve accuracy of fire simulations in earth system models of Pliocene climate.

5. CONCLUSION

The record of high CO₂ supports the hypothesis that Pliocene Arctic terrestrial fossil localities probably represent periods of higher warmth that supported higher productivity. The novel temperature estimates presented here suggest that summer temperatures were considerably warmer during the Pliocene ($\sim 15.4^{\circ}\text{C}$) compared to modern day Eureka, Canada ($\sim 4.1^{\circ}\text{C}$; Fig. 2). This highlights the increasing influence of arctic amplification of temperatures as CO₂ exceeds modern levels. Our reconstruction of the paleovegetation and ecology of this unique site on Ellesmere Island suggests an assemblage similar to forests of the western margins of North America and eastern Fennoscandia. The evidence of recurrent fire and concurrent changes in taxonomic composition suggests that fire played an active role in Pliocene Arctic forests, shaping the environment as it does in the boreal forest today. The importance of fire in the modern boreal forest suggests that fire may have had direct and indirect impacts on Earth's radiative budget at high

Deleted:

Deleted: Matthews and Fyles (2000) similarly indicated that the Pliocene BP environment was characterized by an open larch dominated forest-tundra environment, sharing most species in common with those now found in three regions, including central Alaska to Washington in western North America, the region centered around the Canadian/US border in eastern North America, as well as Fennoscandia in Europe (Fig 7a). Wildfire is a key driver of ecological processes in modern boreal forests (Flannigan et al., 2009; Ryan, 2002), and although historically rare, is becoming more frequent in the tundra in recent years (Mack et al., 2011). The modern increase in fire frequency is likely as a consequence of atmospheric CO₂ driven climate warming and feedbacks such as reduced sea ice extent (Hu et al., 2010), because the probability of fire is highest where temperature and moisture are conducive to growth and drying of fuels followed by conditions that favor ignition (Whitman et al., 2015). Young et al. (2017) confirmed the importance of summer warmth and moisture availability patterns in predicting fire across Alaska, highlighting a July temperature of $\sim 13.5^{\circ}\text{C}$ as a key threshold for fire across Alaska.

—The abundance of charcoal at BP demonstrates that climatic conditions were conducive for ignition and that sufficient biomass available for combustion existed across the landscape. Mean summer temperatures at BP likely exceeded the $\sim 13.5^{\circ}\text{C}$ threshold (Young et al., 2017) that drastically increases the chance of wildfire as demonstrated here from brGDGT derived temperatures and corroborated by previous studies with a seasonal component (Csank et al., 2011b; Fletcher et al., 2017). An increase in atmospheric convection has been simulated in response to diminished sea-ice during warmer intervals (Abbot and Tziperman, 2008), but this study did not confirm if this increase in atmospheric convection was sufficient to cause lightning ignitions. An alternative ignition source for combustion of biomass on Ellesmere Island during the Pliocene is coal seam fires, which have been documented to be burning at this time (Estrada et al., 2009). However, given the interaction of summer warmth and ignition by lightning within the same climate range as posited for BP, we consider lightning the most likely source of ignition for Pliocene fires in the High Arctic.

—Fire return intervals cannot be calculated from the BP charcoal counts due to the absence of a satisfactory age-depth model and discontinuous sampling. As strong interactions are observed between fire regime and ecosystem assemblage in the boreal forest (Brown and Giesecke, 2014; Kasischke and Turetsky, 2006), and in response to climate, comparison with modern fire regimes for areas with shared species compositions and climates may inform a potential range of mean fire return interval (MFR).

—The modern area with the most species in common with BP is central northern Alaska (Fig. 7A). The area over which shared species were calculated is largely tundra, but includes the ecotone between tundra and boreal forest. Other zones that share many species with BP are continuous with Alaska down the western coast of North America to the region around the border of Canada and the United States, the eastern coast of North America in the region around the border of Canada and the United States ($\sim 50^{\circ}\text{N}$), and central Fennoscandia. Of these zones, the MST of Alaskan tundra sites ($6-9^{\circ}\text{C}$) are less similar to BP (15.4°C) than $\sim 50^{\circ}\text{N}$ on both western and eastern coastal North American sites and central Fennoscandia ($12-18^{\circ}\text{C}$, Fig. 7B). The eastern coast of North America has higher rainfall during the summer (>270 mm), than the west coast and Alaska (Fig. 7C), which correlates to the timing of western fires. The low summer precipitation for much of the west (<200 mm), is consistent with previously published summer precipitation estimates for BP (~ 190 mm). As a result, the fire regime of the west coast $\sim 50^{\circ}\text{N}$ may be a better analogue for BP. [1]

Deleted: reveals

Deleted: potential

Deleted: and influencing the climate of the Arctic during the Pliocene

latitudes during the Pliocene, although the net impact of the component process remains unknown. Collectively, these reconstructions provide new insights into the paleoclimatology and paleoecology of the Canadian High Arctic, ~3.9 Ma.

Data Availability. The data generated and used in this analysis are available in the supplemental information associated with this article.

Sample Availability. Samples used in this analysis are curated by the Canadian Museum of Nature. Sample numbers used for each analysis are given in the supplemental information (Table S1 and S2).

Supplemental Link. To be provided by Copernicus Publishing

Author Contribution. Conceptualization: A.P.B. with modification by other authors; Methodology: A.P.B., J.G., J.S.S.D., K.J.B., T.F.; Formal analysis: All authors; Investigation: A.P.B., J.G., K.J.B., L.W., T.F.; Resources: A.P.B., J.G., J.S.S.D., K.J.B.; Data curation: A.P.B., J.G., K.J.B., L.W., T.F.; Writing—Original draft: All authors; Writing—Review and editing: All authors; Supervision: A.P.B., J.S.S.D., K.J.B., N.R.; Project administration: A.P.B., N.R., T.F.; Funding acquisition: A.P.B., J.G., J.S.S.D., K.J.B., N.R., T.F. (Definitions as per the CRediT Taxonomy)

Competing interests. The authors declare that they have no conflict of interest

Acknowledgements. This work was funded by NSF Polar Programs to A.P.B.; National Geographic Committee for Research and Exploration Grant (9912-16) and Endeavour Research Fellowship (5928-2017) to T.F.; National Geographic Explorer Grant (7902-05), [NSERC Discovery Grant \(312193\)](#), and The W. Garfield Weston Foundation grant to N.R.; student travel (N.R. supervised) was supported by the Northern Scientific Training Program (NSTP) from the government of Canada; an NSERC Discovery Grant (239961) with Northern Supplement (362148) to J.C.G.; Natural Resources Canada (SO-03 PA 3.1 Forest Disturbances Wildland Fire) to K.J.B.; the European Research Council under the European Union's Seventh Framework Programme (FP7/2007-2013) / ERC grant agreement n° [226600], and funding from the Netherlands Earth System Science Center (NESSC) through a gravitation grant (NWO 024.002.001) from the Dutch Ministry for Education, Culture and Science to J.S.S.D.

Alice Telka (Paleotek Services) identified and prepared macrofossil plants for the CO₂ analysis. We are also grateful to Nicholas Conder ([Canadian Forest Service](#)) who assisted with sample preparation for the vegetation/fire reconstruction. We also acknowledge the 2006, 2010 and 2012 field teams including D. Finney (Environment Canada), H. Larson (McGill University), M. Vavrek (McGill University), A. Dececchi (McGill University), W.T. Mitchell (Carleton University), R. Smith (University of Saskatchewan), and C. Schröder-Adams (Carleton University). The field research was supported by a paleontology permit from the Government of Nunavut, CLEY (D.R. Stenton, J. Ross) and with the permission of Qikiqtani Inuit Association, especially Grise Fiord (Nunavut).

Deleted: Alterations to Earth's surface and atmospheric radiative budget as a result of fire may help reconcile the gap between high latitude temperature estimates observed from proxies and simulated from models as the impact of these processes are better characterized.

Deleted: Our results further support that near future climate forcing from CO₂ concentrations not experienced for over 3 million years will likely cause a dramatic shift in the climate and ecosystems of the Arctic.

Deleted: G

Deleted: s

Deleted: Royal Ontario Museum

Deleted: Queens University

Logistic support was provided by the Polar Continental Shelf Program (M. Bergmann, B. Hyrcyk, B. Hough, M. Kristjanson, T. McConaghy, J. MacGregor and the PCSP team).

References

- Abbot, D. S. and Tziperman, E.: Sea ice, high-latitude convection, and equable climates, *Geophysical Research Letters*, 35, 2008.
- Auclair, A. N.: Postfire regeneration of plant and soil organic pools in a *Picea mariana*–*Cladonia stellaris* ecosystem, *Canadian Journal of Forest Research*, 15, 279–291, 1985.
- Ballantyne, A. P., Axford, Y., Miller, G. H., Otto-Bliesner, B. L., Rosenbloom, N., and White, J. W.: The amplification of Arctic terrestrial surface temperatures by reduced sea-ice extent during the Pliocene, *Palaeogeography, Palaeoclimatology, Palaeoecology*, 386, 59–67, 2013.
- Ballantyne, A. P., Greenwood, D. R., Sinninghe Damsté, J. S., Csank, A. Z., Eberle, J. J., and Rybczynski, N.: Significantly warmer Arctic surface temperatures during the Pliocene indicated by multiple independent proxies, *Geology*, 38, 603–606, 2010.
- Ballantyne, A. P., Rybczynski, N., Baker, P. A., Harington, C. R., and White, D.: Pliocene Arctic temperature constraints from the growth rings and isotopic composition of fossil larch, *Palaeogeography, Palaeoclimatology, Palaeoecology*, 242, 188–200, 2006.
- Bauska, T. K., Baggenstos, D., Brook, E. J., Mix, A. C., Marcott, S. A., Petrenko, V. V., Schaefer, H., Severinghaus, J. P., and Lee, J. E.: Carbon isotopes characterize rapid changes in atmospheric carbon dioxide during the last deglaciation, *Proceedings of the National Academy of Sciences*, 2016. 201513868, 2016.
- Bendle, J. A., Weijers, J. W., Maslin, M. A., Sinninghe Damsté, J. S., Schouten, S., Hopmans, E. C., Boot, C. S., and Pancost, R. D.: Major changes in glacial and Holocene terrestrial temperatures and sources of organic carbon recorded in the Amazon fan by tetraether lipids, *Geochemistry, Geophysics, Geosystems*, 11, 2010.
- Berg, E. E. and Chapin III, F. S.: Needle loss as a mechanism of winter drought avoidance in boreal conifers, *Canadian Journal of Forest Research*, 24, 1144–1148, 1994.
- Bergeron, Y.: The influence of island and mainland lakeshore landscapes on boreal forest fire regimes, *Ecology*, 72, 1980–1992, 1991.
- Bergeron, Y., Cyr, D., Drever, C. R., Flannigan, M., Gauthier, S., Kneeshaw, D., Lauzon, È., Leduc, A., Goff, H. L., Lesieur, D., and Logan, K.: Past, current, and future fire frequencies in Quebec's commercial forests: implications for the cumulative effects of harvesting and fire on age-class structure and natural disturbance-based management, *Canadian Journal of Forest Research*, 36, 2737–2744, 2006.
- Bonan, G.: *Ecological climatology: concepts and applications*, Cambridge University Press, 2015.
- Bouchard, M., Pothier, D., and Gauthier, S.: Fire return intervals and tree species succession in the North Shore region of eastern Quebec, *Canadian Journal of Forest Research*, 38, 1621–1633, 2008.
- Brigham-Grette, J. and Carter, L. D.: Pliocene Marine Transgressions of Northern Alaska: Circumarctic Correlations and Paleoclimatic Interpretations, *Arctic*, 45, 74–89, 1992.

Deleted: Bonan, G., B.: *Forests and Climate Change: Forcings, Feedbacks, and the Climate Benefits of Forests*, *Science*, 320, 1444–1449, 2008.

Brown, K. J. and Giesecke, T.: Holocene fire disturbance in the boreal forest of central Sweden, *Boreas*, 43, 639–651, 2014.

Brown, K. J. and Power, M. J.: Charred particle analyses. In: *Encyclopedia of Quaternary Science*, Elias, S. (Ed.), Elsevier, Amsterdam, 2013.

Brown, M.: Fire and Ice: Fire Severity and Future Flammability in Alaskan Black Spruce Forests, *Fire Science Brief*, 2008. 1–6, 2008.

Busher, P. E.: Food Caching Behavior of Beavers (*Castor canadensis*): Selection and Use of Woody Species, *The American Midland Naturalist*, 135, 343–348, 1996.

Clymo, R. S.: The Origin of Acidity in Sphagnum Bogs, *The Bryologist*, 67, 427–431, 1964.

Côté, M., Ferron, J., and Gagnon, R.: Impact of seed and seedling predation by small rodents on early regeneration establishment of black spruce, *Canadian Journal of Forest Research*, 33, 2362–2371, 2003.

Csank, A. Z., Patterson, W. P., Eglington, B. M., Rybczynski, N., and Basinger, J. F.: Climate variability in the Early Pliocene Arctic: Annually resolved evidence from stable isotope values of sub-fossil wood, Ellesmere Island, Canada, *Palaeogeography, Palaeoclimatology, Palaeoecology*, 308, 339–349, 2011a.

Csank, A. Z., Tripathi, A. K., Patterson, W. P., Eagle, R. A., Rybczynski, N., Ballantyne, A. P., and Eiler, J. M.: Estimates of Arctic land surface temperatures during the early Pliocene from two novel proxies, *Earth and Planetary Science Letters*, 304, 291–299, 2011b.

de Groot, W. J., Cantin, A. S., Flannigan, M. D., Soja, A. J., Gowman, L. M., and Newbery, A.: A comparison of Canadian and Russian boreal forest fire regimes, *Forest Ecology and Management*, 294, 23–34, 2013.

de Groot, W. J., Thomas, P. A., and Wein, R. W.: *Betula nana* L. and *Betula glandulosa* Michx., *Journal of Ecology*, 85, 241–264, 1997.

De Jonge, C., Hopmans, E. C., Stadnitskaia, A., Rijpstra, W. I. C., Hofland, R., Tegelaar, E., and Sinninghe Damsté, J. S.: Identification of novel penta- and hexamethylated branched glycerol dialkyl glycerol tetraethers in peat using HPLC–MS 2, GC–MS and GC–SMB–MS, *Organic geochemistry*, 54, 78–82, 2013.

De Jonge, C., Hopmans, E. C., Zell, C. I., Kim, J.-H., Schouten, S., and Sinninghe Damsté, J. S.: Occurrence and abundance of 6-methyl branched glycerol dialkyl glycerol tetraethers in soils: Implications for palaeoclimate reconstruction, *Geochimica et Cosmochimica Acta*, 141, 97–112, 2014.

De Jonge, C., Stadnitskaia, A., Hopmans, E. C., Cherkashov, G., Fedotov, A., Streletskaia, I. D., Vasiliev, A. A., and Sinninghe Damsté, J. S.: Drastic changes in the distribution of branched tetraether lipids in suspended matter and sediments from the Yenisei River and Kara Sea (Siberia): Implications for the use of brGDGT-based proxies in coastal marine sediments, *Geochimica et Cosmochimica Acta*, 165, 200–225, 2015.

de Lafontaine, G. and Payette, S.: Shifting zonal patterns of the southern boreal forest in eastern Canada associated with changing fire regime during the Holocene, *Quaternary Science Reviews*, 30, 867–875, 2011.

Dee, D. P., Uppala, S. M., Simmons, A. J., Berrisford, P., Poli, P., Kobayashi, S., Andrae, U., Balmaseda, M. A., Balsamo, G., and Bauer, P.: The ERA-Interim reanalysis: Configuration and performance of the data assimilation system, *Quarterly Journal of the Royal Meteorological Society*, 137, 553–597, 2011.

Deleted: Brown, D., Jorgenson, M. T., Douglas, T. A., Romanovsky, V. E., Kielland, K., Hiemstra, C., Euskirchen, E. S., and Ruess, R. W.: Interactive effects of wildfire and climate on permafrost degradation in Alaskan lowland forests, *Journal of Geophysical Research: Biogeosciences*, 120, 1619–1637, 2015.

Deleted: Chapin III, F. S., Sturm, M., Serreze, M. C., McFadden, J. P., Key, J. R., Lloyd, A. H., McGuire, A. D., Rupp, T. S., Lynch, A. H., Schimel, J. P., Beringer, J., Chapman, W. L., Epstein, H. E., Euskirchen, E. S., Hinzman, L. D., Jia, G., Ping, C. L., Tape, K. D., Thompson, C. D. C., Walker, D. A., and Welker, J. M.: Role of Land-Surface Changes in Arctic Summer Warming, *Science*, 310, 657–660, 2005.

Diefendorf, A. F., Mueller, K. E., Wing, S. L., Koch, P. L. and Freeman, K. H.: Global patterns in leaf $\delta^{13}C$ discrimination and implications for studies of past and future climate. *Proceedings of the National Academy of Sciences*, 107, 5738–5743, 2010.

Dowsett, H., Dolan, A., Rowley, D., Pound, M., Salzmann, U., Robinson, M., Chandler, M., Foley, K., and Haywood, A.: The PRISM4 (mid-Piacenzian) palaeoenvironmental reconstruction, *Climate of the Past*, doi: doi:10.5194/cp-12-1519-2016, 2016. 2016.

Dowsett, H. J., Cronin, T. M., Poore, R. Z., Thompson, R. S., Whatley, R. C., and Wood, A. M.: Micropaleontological evidence for increased meridional heat transport in the North Atlantic Ocean during the Pliocene, *Science*, 258, 1133–1136, 1992.

Dowsett, H. J., Robinson, M. M., Haywood, A. M., Hill, D. J., Dolan, A. M., Stoll, D. K., Chan, W. L., Abe-Ouchi, A., Chandler, M. A., and Rosenbloom, N. A.: Assessing confidence in Pliocene sea surface temperatures to evaluate predictive models, *Nature Climate Change*, 2, 365–371, 2012.

Estrada, S., Piepjohn, K., Frey, M. J., Reinhardt, L., Andrulleit, H., and von Gosen, W.: Pliocene coal-seam fires on southern Ellesmere Island, Canadian Arctic, *Neues Jahrbuch für Geologie und Paläontologie - Abhandlungen*, 251, 33–52, 2009.

Farquhar, G. D., Ehleringer, J. R., and Hubick, K. T.: Carbon isotope discrimination and photosynthesis, *Annual Review of Plant Biology*, 40, 503–537, 1989.

Feng, R., Otto-Bliesner, B., Fletcher, T., Ballantyne, A., and Brady, E.: Contributions to Pliocene Arctic warmth from removal of anthropogenic aerosol and enhanced forest fire emissions, San Francisco, USA. 2016, PP33A-2344.

Feng, R., Otto-Bliesner, B. L., Fletcher, T. L., Tabor, C. R., Ballantyne, A. P., and Brady, E. C.: Amplified Late Pliocene terrestrial warmth in northern high latitudes from greater radiative forcing and closed Arctic Ocean gateways, *Earth and Planetary Science Letters*, 466, 129–138, 2017.

Flannigan, M., Stocks, B., Turetsky, M., and Wotton, M.: Impacts of climate change on fire activity and fire management in the circumboreal forest, *Global Change Biology*, 15, 549–560, 2009.

Fletcher, B. J., Brentnall, S. J., Anderson, C. W., Berner, R. A., and Beerling, D. J.: Atmospheric carbon dioxide linked with Mesozoic and early Cenozoic climate change, *Nature Geoscience*, 1, 43–48, 2008.

Fletcher, T., Feng, R., Telka, A. M., Matthews, J. V., and Ballantyne, A.: Floral dissimilarity and the influence of climate in the Pliocene High Arctic: Biotic and abiotic influences on five sites on the Canadian Arctic Archipelago, *Frontiers in Ecology and Evolution*, 5, 19, 2017.

Foster, L. C., Pearson, E. J., Juggins, S., Hodgson, D. A., Saunders, K. M., Verleyen, E., and Roberts, S. J.: Development of a regional glycerol dialkyl glycerol tetraether (GDGT)–temperature calibration for Antarctic and sub-Antarctic lakes, *Earth and Planetary Science Letters*, 433, 370–379, 2016.

[Foster, G. L., Royer, D. L., and Lunt, D. J.: Future climate forcing potentially without precedent in the last 420 million years, *Nature Communications*, 8, 14845, 2017.](#)

[Francis, J. and Skific, N.: Evidence linking rapid Arctic warming to mid-latitude weather patterns, *Philosophical Transactions of the Royal Society A: Mathematical, Physical and Engineering Sciences*, 373, 1–12, 2015.](#)

Deleted: Fisher, J. P., Estop-Aragónés, C., Thierry, A., Charman, D. J., Wolfe, S. A., Hartley, I. P., Merton, J. B., Williams, M., and Phoenix, G. K.: The influence of vegetation and soil characteristics on active-layer thickness of permafrost soils in boreal forest, *Global Change Biology*, 2016. 2016.

GBIF.org: GBIF Occurrence Download (Beaver Pond extant species) <http://doi.org/10.15468/dl.ertiqj> 1st February 2017.

GBIF.org: GBIF Occurrence Download (*Betula*) <https://doi.org/10.15468/dl.akxgp5> 11th May 2018a.

GBIF.org: GBIF Occurrence Download (*Larix*) <https://doi.org/10.15468/dl.mfhnci> 11th May 2018b.

GBIF.org: GBIF Occurrence Download (*Picea*) <https://doi.org/10.15468/dl.wi7jdc> 11th May 2018c.

GBIF.org: GBIF Occurrence Download (*Pinus*) <https://doi.org/10.15468/dl.vwfjj2> 11th May 2018d.

Global View-CO₂: Cooperative Global Atmospheric Data Integration Project. 2013, updated annually. Multi-laboratory compilation of synchronized and gap-filled atmospheric carbon dioxide records for the period 1979-2012. Compiled by NOAA Global Monitoring Division: Boulder, Colorado, U.S.A, 2013.

Greene, G. A. and Daniels, L. D.: Spatial interpolation and mean fire interval analyses quantify historical mixed-severity fire regimes, *International Journal of Wildland Fire*, 26, 136–147, 2017.

Haarberg, O. and Rosell, F.: Selective foraging on woody plant species by the Eurasian beaver (*Castor fiber*) in Telemark, Norway, *Journal of Zoology*, 270, 201–208, 2006.

Haywood, A. M., Dowsett, H. J., and Dolan, A. M.: Integrating geological archives and climate models for the mid-Pliocene warm period, *Nature communications*, 7, 1–14, 2016.

Higuera, P., Barnes, J. L., Chipman, M. L., Urban, M., and Hu, F. S.: The burning tundra: A look back at the last 6,000 years of fire in the Noatak National Preserve, Northwestern Alaska, *Alaska Park Science*, 10, 37–41, 2011.

Higuera, P. E., Brubaker, L. B., Anderson, P. M., Hu, F. S., and Brown, T. A.: Vegetation mediated the impacts of postglacial climate change on fire regimes in the south-central Brooks Range, Alaska, *Ecological Monographs*, 79, 201–219, 2009.

Hijmans, R. J., Cameron, S. E., Parra, J. L., Jones, P. G., and Jarvis, A.: Very high resolution interpolated climate surfaces for global land areas, *International Journal of Climatology*, 25, 1965–1978, 2005.

Hönisch, B., Hemming, N. G., Archer, D., Siddall, M., and McManus, J. F.: Atmospheric Carbon Dioxide Concentration Across the Mid-Pleistocene Transition, *Science*, 324, 1551–1554, 2009.

Hopmans, E. C., Schouten, S., and Sinninghe Damsté, J. S.: The effect of improved chromatography on GDGT-based palaeoproxies, *Organic Geochemistry*, 93, 1–6, 2016.

Hu, F. S., Higuera, P. E., Walsh, J. E., Chapman, W. L., Duffy, P. A., Brubaker, L. B., and Chipman, M. L.: Tundra burning in Alaska: Linkages to climatic change and sea ice retreat, *Journal of Geophysical Research: Biogeosciences*, 115, 2010.

Huber, M.: A Hotter Greenhouse?, *Science*, 321, 353–354, 2008.

Huguet, C., Hopmans, E. C., Febo-Ayala, W., Thompson, D. H., Sinninghe Damsté, J. S., and Schouten, S.: An improved method to determine the absolute abundance of glycerol dibiphytanyl glycerol tetraether lipids, *Organic Geochemistry*, 37, 1036–1041, 2006.

Hwang, Y. T., Frierson, D. M., and Kay, J. E.: Coupling between Arctic feedbacks and changes in poleward energy transport, *Geophysical Research Letters*, 38, 2011.

Jacquelyn, K. S., Adrianna, C. F., Herman, H. S., Amanda, H.-H., Alexander, K., Tatiana, L., Dmitry, E., and Elena, S.: Fire disturbance and climate change: implications for Russian forests, *Environmental Research Letters*, 12, 035003, 2017.

Jenkins, S. H.: Seasonal and year-to-year differences in food selection by beavers, *Oecologia*, 44, 112–116, 1979.

Johnstone, J. F., Chapin, F. S., Hollingsworth, T. N., Mack, M. C., Romanovsky, V., and Turetsky, M.: Fire, climate change, and forest resilience in interior Alaska, *Canadian Journal of Forest Research*, 40, 1302–1312, 2010a.

Johnstone, J. F., Hollingsworth, T. N., Chapin, F. S., and Mack, M. C.: Changes in fire regime break the legacy lock on successional trajectories in Alaskan boreal forest, *Global Change Biology*, 16, 1281–1295, 2010b.

Johnstone, J. F. and Kasischke, E. S.: Stand-level effects of soil burn severity on postfire regeneration in a recently burned black spruce forest, *Canadian Journal of Forest Research*, 35, 2151–2163, 2005.

Jones, P. D. and Moberg, A.: Hemispheric and large-scale surface air temperature variations: An extensive revision and an update to 2001, *Journal of Climate*, 16, 206–223, 2003.

Kasischke, E. S. and Turetsky, M. R.: Recent changes in the fire regime across the North American boreal region—spatial and temporal patterns of burning across Canada and Alaska, *Geophysical research letters*, 33, 2006.

Kasischke, E. S., Turetsky, M. R., Ottmar, R. D., French, N. H., Hoy, E. E., and Kane, E. S.: Evaluation of the composite burn index for assessing fire severity in Alaskan black spruce forests, *International Journal of Wildland Fire*, 17, 515–526, 2008.

Kasischke, E. S., Williams, D., and Barry, D.: Analysis of the patterns of large fires in the boreal forest region of Alaska, *International Journal of Wildland Fire*, 11, 131–144, 2002.

Kharuk, V. I., Dvinskaya, M. L., Petrov, I. A., Im, S. T., and Ranson, K. J.: Larch forests of Middle Siberia: long-term trends in fire return intervals, *Regional Environmental Change*, doi: 10.1007/s10113-016-0964-9, 2016. 1–9, 2016.

Kharuk, V. I., Ranson, K. J., Dvinskaya, M. L., and Im, S. T.: Wildfires in northern Siberian larch dominated communities, *Environmental Research Letters*, 6, 045208, 2011.

Kobayashi, M., Nemilostiv, Y. P., Zyryanova, O. A., Kajimoto, T., Matsuura, Y., Yoshida, T., Satoh, F., Sasa, K., and Koike, T.: Regeneration after forest fires in mixed conifer broad-leaved forests of the Amur region in far eastern Russia: the relationship between species specific traits against fire and recent fire regimes, *Eurasian Journal of Forest Research*, 10, 51–58, 2007.

Kooijman, A. and Westhoff, V.: Variation in habitat factors and species composition of *Scorpidium scorpioides* communities in NW-Europe, *Plant Ecology*, 117, 133–150, 1995.

Kooijman, A. M. and Paulissen, M. P. C. P.: Higher acidification rates in fens with phosphorus enrichment, *Applied Vegetation Science*, 9, 205–212, 2006.

Leavitt, S. W. and Danzer, S. R.: Method for batch processing small wood samples to holocellulose for stable-carbon isotope analysis, *Analytical Chemistry*, 65, 87–89, 1993.

Lifton, N., Sato, T., and Dunai, T. J.: Scaling in situ cosmogenic nuclide production rates using analytical approximations to atmospheric cosmic-ray fluxes, *Earth and Planetary Science Letters*, 386, 149–160, 2014.

Lisiecki, L. E. and Raymo, M. E.: A Plio-Pleistocene stack of 57 globally distributed benthic $\delta^{18}\text{O}$ records, *Paleoceanography*, 20, 2005.

Loomis, S. E., Russell, J. M., Ladd, B., Street-Perrott, F. A., and Sinninghe Damsté, J. S.: Calibration and application of the branched GDGT temperature proxy on East African lake sediments, *Earth and Planetary Science Letters*, 357, 277–288, 2012.

Lorimer, C. G.: The Presettlement Forest and Natural Disturbance Cycle of Northeastern Maine, *Ecology*, 58, 139–148, 1977.

Luthi, D., Le Floch, M., Bereiter, B., Blunier, T., Barnola, J.-M., Siegenthaler, U., Raynaud, D., Jouzel, J., Fischer, H., Kawamura, K., and Stocker, T. F.: High-resolution carbon dioxide concentration record 650,000–800,000 years before present, *Nature*, 453, 379–382, 2008.

Lynch, J. A., Clark, J. S., Bigelow, N. H., Edwards, M. E., and Finney, B. P.: Geographic and temporal variations in fire history in boreal ecosystems of Alaska, *Journal of Geophysical Research: Atmospheres*, 107, FFR 8-1–FFR 8-17, 2002.

Mack, M. C., Bret-Harte, M. S., Hollingsworth, T. N., Jandt, R. R., Schuur, E. A. G., Shaver, G. R., and Verbyla, D. L.: Carbon loss from an unprecedented Arctic tundra wildfire, *Nature*, 475, 489–492, 2011.

Marshall, J., Armour, K. C., Scott, J. R., Kostov, Y., Hausmann, U., Ferreira, D., Shepherd, T. G., and Bitz, C. M.: The ocean's role in polar climate change: asymmetric Arctic and Antarctic responses to greenhouse gas and ozone forcing, *Philosophical Transactions of the Royal Society of London A: Mathematical, Physical and Engineering Sciences*, 372, 20130040, 2014.

Martinez-Boti, M. A., Foster, G. L., Chalk, T. B., Rohling, E. J., Sexton, P. F., Lunt, D. J., Pancost, R. D., Badger, M. P. S., and Schmidt, D. N.: Plio-Pleistocene climate sensitivity evaluated using high-resolution CO₂ records, *Nature*, 518, 49–54, 2015.

Matthews Jr, J. V. and Ovenden, L. E.: Late Tertiary plant macrofossils from localities in Arctic/sub- Arctic North America: a review of the data, *Arctic*, 43, 364–392, 1990.

Matthews, J. V. J. and Fyles, J. G.: Late Tertiary plant and arthropod fossils from the High Terrace Sediments on the Fosheim Peninsula of Ellesmere Island (Northwest Territories, District of Franklin), *Geological Survey of Canada, Bulletin*, 529, 295–317, 2000.

Mattson, M. D.: Acid lakes and rivers. In: *Environmental Geology*, Springer Netherlands, Dordrecht, 1999.

McAndrews, J. H., Berti, A. A., and Norris, G.: Key to the Quaternary pollen and spores of the Great Lakes region, 1973. 1973.

Ménot, G. and Burns, S. J.: Carbon isotopes in ombrogenic peat bog plants as climatic indicators: calibration from an altitudinal transect in Switzerland, *Organic Geochemistry*, 32, 233–245, 2001.

Miller, G. H., Alley, R. B., Brigham-Grette, J., Fitzpatrick, J. J., Polyak, L., Serreze, M. C., and White, J. W. C.: Arctic amplification: can the past constrain the future?, *Quaternary Science Reviews*, 29, 1779–1790, 2010.

Mitchell, W. T., Rycbczynski, N., Schröder-Adams, C., Hamilton, P. B., Smith, R., and Douglas, M.: Stratigraphic and Paleoenvironmental Reconstruction of a Mid-Pliocene Fossil Site in the High Arctic (Ellesmere Island, Nunavut): Evidence of an Ancient Peatland with Beaver Activity, *Arctic*, 69, 185–204, 2016.

Moore, P. D., Webb, J. A., and Collison, M. E.: Pollen analysis, Blackwell Scientific Publications, Oxford, 1991.

Deleted: McConnell, J. R., Edwards, R., Kok, G. L., Flanner, M. G., Zender, C. S., Saltzman, E. S., Banta, J. R., Pasteris, D. R., Carter, M. M., and Kahl, J. D. W.: 20th-century industrial black carbon emissions altered arctic climate forcing, *Science*, 317, 1381–1384, 2007.

Naafs, B., Inglis, G., Zheng, Y., Amesbury, M., Biester, H., Bindler, R., Blewett, J., Burrows, M., del Castillo Torres, D., and Chambers, F. M.: Introducing global peat-specific temperature and pH calibrations based on brGDGT bacterial lipids, *Geochimica et Cosmochimica Acta*, 208, 285–301, 2017.

Niemann, H., Stadnitskaia, A., Wirth, S., Gilli, A., Anselmetti, F., Sinninghe Damsté, J., Schouten, S., Hopmans, E., and Lehmann, M.: Bacterial GDGTs in Holocene sediments and catchment soils of a high Alpine lake: application of the MBT/CBT-paleothermometer, *Climate of the Past*, 8, 889–906, 2012.

Niklasson, M. and Drakenberg, B.: A 600-year tree-ring fire history from Norra Kvills National Park, southern Sweden: implications for conservation strategies in the hemiboreal zone, *Biological Conservation*, 101, 63–71, 2001.

Niklasson, M. and Granström, A.: Fire in Sweden – History, Research, Prescribed Burning and Forest Certification, *International Forest Fire News*, 30, 80–83, 2004.

Niklasson, M. and Granström, A.: Numbers and sizes of fires: Long-term spatially explicit fire history in a Swedish boreal landscape, *Ecology*, 81, 1484–1499, 2000.

Otto-Bliesner, B. L. and Upchurch Jr, G. R.: Vegetation-induced warming of high-latitude regions during the Late Cretaceous period, *Nature*, 385, 804, 1997.

Pagani, M., Liu, Z., LaRiviere, J., and Ravelo, A. C.: High Earth-system climate sensitivity determined from Pliocene carbon dioxide concentrations, *Nature Geoscience*, 3, 27–30, 2010.

Pearson, E. J., Juggins, S., Talbot, H. M., Weckström, J., Rosén, P., Ryves, D. B., Roberts, S. J., and Schmidt, R.: A lacustrine GDGT-temperature calibration from the Scandinavian Arctic to Antarctic: Renewed potential for the application of GDGT-paleothermometry in lakes, *Geochimica et Cosmochimica Acta*, 75, 6225–6238, 2011.

Peterse, F., Prins, M. A., Beets, C. J., Troelstra, S. R., Zheng, H., Gu, Z., Schouten, S., and Sinninghe Damsté, J. S.: Decoupled warming and monsoon precipitation in East Asia over the last deglaciation, *Earth and Planetary Science Letters*, 301, 256–264, 2011.

Powers, L. A., Werne, J. P., Johnson, T. C., Hopmans, E. C., Sinninghe Damsté, J. S., and Schouten, S.: Crenarchaeotal membrane lipids in lake sediments: A new paleotemperature proxy for continental paleoclimate reconstruction?, *Geology*, 32, 613–616, 2004.

R Core Team: R: A language and environment for statistical computing. R Foundation for Statistical Computing, Vienna, Austria, 2016.

Racine, C. H., Johnson, L. A., and Viereck, L. A.: Patterns of Vegetation Recovery after Tundra Fires in Northwestern Alaska, U.S.A., *Arctic and Alpine Research*, 19, 461–469, 1987.

Ravelo, A. C., Andreasen, D. H., Lyle, M., Lyle, A. O., and Wara, M. W.: Regional climate shifts caused by gradual global cooling in the Pliocene epoch, *Nature*, 429, 263–267, 2004.

Raymo, M. E., Lisiecki, L. E., and Nisancioglu, K. H.: Plio-Pleistocene ice volume, Antarctic climate, and the global $\delta^{18}\text{O}$ record, *Science*, 313, 492–495, 2006.

Robinson, M. M.: New Quantitative Evidence of Extreme Warmth in the Pliocene Arctic, *Stratigraphy*, 6, 265–275, 2009.

Rogers, B. M., Soja, A. J., Goulden, M. L., and Randerson, J. T.: Influence of tree species on continental differences in boreal fires and climate feedbacks, *Nature Geoscience*, 8, 228–234, 2015.

Deleted: Randerson, J., Liu, H., Flanner, M., Chambers, S., Jin, Y., Hess, P., Pfister, G., Mack, M., Treseder, K., and Welp, L.: The impact of boreal forest fire on climate warming, *Science*, 314, 1130–1132, 2006.

Rovere, A., Raymo, M. E., Mitrovica, J. X., Hearty, P. J., O'Leary, M. J., and Inglis, J. D.: The Mid-Pliocene sea-level conundrum: Glacial isostasy, eustasy and dynamic topography, *Earth and Planetary Science Letters*, 387, 27–33, 2014.

Royer, D. L.: CO₂-forced climate thresholds during the Phanerozoic, *Geochimica et Cosmochimica Acta*, 70, 5665–5675, 2006.

Royer, D. L., Berner, R. A., and Park, J.: Climate sensitivity constrained by CO₂ concentrations over the past 420 million years, *Nature*, 446, 530–532, 2007.

Royles, J., Horwath, A. B., and Griffiths, H.: Interpreting bryophyte stable carbon isotope composition: Plants as temporal and spatial climate recorders, *Geochemistry, Geophysics, Geosystems*, 15, 1462–1475, 2014.

Russell, J. M., Hopmans, E. C., Loomis, S. E., Liang, J., and Sinninghe Damsté, J. S.: Distributions of 5- and 6-methyl branched glycerol dialkyl glycerol tetraethers (brGDGTs) in East African lake sediment: Effects of temperature, pH, and new lacustrine paleotemperature calibrations, *Geochimica et Cosmochimica Acta*, 117, 56–69, 2018.

Ryan, K. C.: Dynamic interactions between forest structure and fire behavior in boreal ecosystems, *Silva Fennica*, 36, 13–39, 2002.

Rybczynski, N., Gosse, J. C., Richard Harington, C., Wogelius, R. A., Hidy, A. J., and Buckley, M.: Mid-Pliocene warm-period deposits in the High Arctic yield insight into camel evolution, *Nature Communications*, 4, 1–9, 2013.

Salzmänn, U., Dolan, A. M., Haywood, A. M., Chan, W.-L., Voss, J., Hill, D. J., Abe-Ouchi, A., Otto-Bliesner, B., Bragg, F. J., and Chandler, M. A.: Challenges in quantifying Pliocene terrestrial warming revealed by data-model discord, *Nature Climate Change*, 3, 969, 2013.

Salzmänn, U., Haywood, A. M., Lunt, D., Valdes, P., and Hill, D.: A new global biome reconstruction and data-model comparison for the middle Pliocene, *Global Ecology and Biogeography*, 17, 432–447, 2008.

Schlesinger, W. H. and Vengosh, A.: Global boron cycle in the Anthropocene, *Global Biogeochemical Cycles*, 30, 219–230, 2016.

Seki, O., Foster, G. L., Schmidt, D. N., Mackensen, A., Kawamura, K., and Pancost, R. D.: Alkenone and boron-based Pliocene *p*CO₂ records, *Earth and Planetary Science Letters*, 292, 201–211, 2010.

Shellito, C. J., Lamarque, J.-F., and Sloan, L. C.: Early Eocene Arctic climate sensitivity to *p*CO₂ and basin geography, *Geophysical Research Letters*, 36, 2009.

Sinninghe Damsté, J. S.: Spatial heterogeneity of sources of branched tetraethers in shelf systems: The geochemistry of tetraethers in the Berau River delta (Kalimantan, Indonesia), *Geochimica et Cosmochimica Acta*, 186, 13–31, 2016.

[Sinninghe Damsté J.S., Rijpstra W.I.C., Foesel B.U., Huber K., Overmann J., Nakagawa S., Joong Jae Kim, Dunfield P.F., Dedysh S.N., Villanueva L. \(2018\) An overview of the occurrence of ether- and ester-linked iso-diabolic acid membrane lipids in microbial cultures of the Acidobacteria: Implications for brGDGT palaeoproxies for temperature and pH. *Organic Geochemistry*, 124, 63–76.](#)

Sinninghe Damsté, J. S., Rijpstra, W. I. C., Hopmans, E. C., Foesel, B. U., Wüst, P. K., Overmann, J., Tank, M., Bryant, D. A., Dunfield, P. F., Houghton, K., and Stott, M. B.: Ether- and Ester-Bound iso-Diabolic Acid and Other Lipids in Members of Acidobacteria Subdivision 4, *Applied and Environmental Microbiology*, 80, 5207–5218, 2014.

Sinninghe Damsté, J. S., Rijpstra, W. I. C., Hopmans, E. C., Weijers, J. W., Foesel, B. U., Overmann, J., and Dedys, S. N.: 13, 16-Dimethyl octacosanedioic acid (iso-diabolic acid), a common membrane-spanning lipid of Acidobacteria subdivisions 1 and 3, *Applied and Environmental Microbiology*, 77, 4147–4154, 2011.

Skrzypek, G., Kałużny, A., Wojtuń, B., and Jędrysek, M.-O.: The carbon stable isotopic composition of mosses: A record of temperature variation, *Organic Geochemistry*, 38, 1770–1781, 2007.

Stap, L. B., de Boer, B., Ziegler, M., Bintanja, R., Lourens, L. J., and van de Wal, R. S.: CO₂ over the past 5 million years: Continuous simulation and new $\delta^{11}\text{B}$ -based proxy data, *Earth and Planetary Science Letters*, 439, 1–10, 2016.

Swann, A. L., Fung, I. Y., Levis, S., Bonan, G. B., and Doney, S. C.: Changes in Arctic vegetation amplify high-latitude warming through the greenhouse effect, *Proceedings of the National Academy of Sciences of the United States of America*, 107, 1295–1300, 2010.

Tedford, R. H. and Harington, C. R.: An Arctic mammal fauna from the early Pliocene of North America, *Nature*, 425, 388–390, 2003.

Tripathi, A. K., Roberts, C. D., and Eagle, R. A.: Coupling of CO₂ and Ice Sheet Stability over Major Climate Transitions of the Last 20 Million Years, *Science*, 326, 1394–1397, 2009.

Van Wagner, C. E., Finney, M. A., and Heathcote, M.: Historical fire cycles in the Canadian Rocky Mountain parks, *Forest Science*, 52, 704–717, 2006.

Waite, M. and Sack, L.: Shifts in bryophyte carbon isotope ratio across an elevation \times soil age matrix on Mauna Loa, Hawaii: do bryophytes behave like vascular plants?, *Oecologia*, 166, 11–22, 2011.

Wang, X., Rybczynski, N., Harington, C. R., White, S. C., and Tedford, R. H.: A basal ursine bear (*Protarctos abstrusus*) from the Pliocene High Arctic reveals Eurasian affinities and a diet rich in fermentable sugars, *Scientific reports*, 7, 17722, 2017.

Warden, L., Jung-Hyun, K., Zell, C., Vis, G.-J., de Stigter, H., Bonnín, J., and Sinninghe Damsté, J. S.: Examining the provenance of branched GDGTs in the Tagus River drainage basin and its outflow into the Atlantic Ocean over the Holocene to determine their usefulness for paleoclimate applications, *Biogeosciences*, 13, 5719, 2016.

Weijers, J. W., Schefuß, E., Schouten, S., and Sinninghe Damsté, J. S.: Coupled thermal and hydrological evolution of tropical Africa over the last deglaciation, *Science*, 315, 1701–1704, 2007a.

Weijers, J. W., Schouten, S., van den Donker, J. C., Hopmans, E. C., and Sinninghe Damsté, J. S.: Environmental controls on bacterial tetraether membrane lipid distribution in soils, *Geochimica et Cosmochimica Acta*, 71, 703–713, 2007b.

Weijers, J. W. H., Schouten, S., van den Donker, J. C., Hopmans, E. C., and Sinninghe Damsté, J. S.: Environmental controls on bacterial tetraether membrane lipid distribution in soils, *Geochimica et Cosmochimica Acta*, 71, 703–713, 2007c.

White, J., Ciais, P., Figge, R., Kenny, R., and Markgraf, V.: A high-resolution record of atmospheric CO₂ content from carbon isotopes in peat, *Nature*, 367, 153–156, 1994.

Whitman, E., Batllori, E., Parisien, M. A., Miller, C., Coop, J. D., Krawchuk, M. A., Chong, G. W., and Haire, S. L.: The climate space of fire regimes in north-western North America, *Journal of Biogeography*, 42, 1736–1749, 2015.

- Wright, C. S. and Agee, J. K.: Fire and vegetation history in the eastern Cascade Mountains, Washington, *Ecological Applications*, 14, 443–459, 2004.
- Yang, G., Zhang, C. L., Xie, S., Chen, Z., Gao, M., Ge, Z., and Yang, Z.: Microbial glycerol dialkyl glycerol tetraethers from river water and soil near the Three Gorges Dam on the Yangtze River, *Organic Geochemistry*, 56, 40–50, 2013.
- Yarie, J.: Forest fire cycles and life tables: a case study from interior Alaska, *Canadian Journal of Forest Research*, 11, 554–562, 1981.
- Young, A. M., Higuera, P. E., Duffy, P. A., and Hu, F. S.: Climatic thresholds shape northern high-latitude fire regimes and imply vulnerability to future climate change, *Ecography*, 40, 606–617, 2017.
- Zech, R., Gao, L., Tarozo, R., and Huang, Y.: Branched glycerol dialkyl glycerol tetraethers in Pleistocene loess-paleosol sequences: three case studies, *Organic geochemistry*, 53, 38–44, 2012.
- Zell, C., Kim, J.-H., Moreira-Turcq, P., Abril, G., Hopmans, E. C., Bonnet, M.-P., Sobrinho, R. L., and Sinninghe Damsté, J. S.: Disentangling the origins of branched tetraether lipids and crenarchaeol in the lower Amazon River: Implications for GDGT-based proxies, *Limnology and Oceanography*, 58, 343–353, 2013.
- Zhu, C., Weijers, J. W., Wagner, T., Pan, J.-M., Chen, J.-F., and Pancost, R. D.: Sources and distributions of tetraether lipids in surface sediments across a large river-dominated continental margin, *Organic Geochemistry*, 42, 376–386, 2011.
- Zink, K.-G., Vandergoes, M. J., Mangelsdorf, K., Dieffenbacher-Krall, A. C., and Schwark, L.: Application of bacterial glycerol dialkyl glycerol tetraethers (GDGTs) to develop modern and past temperature estimates from New Zealand lakes, *Organic Geochemistry*, 41, 1060–1066, 2010.

Table 1. Modern and recent Holocene fire return interval reconstructions for the candidate analogous regions considered in this study.

Region	Modern		Reference	Recent Holocene		Reference
Alaskan Tundra	Seward Peninsula	273*	Kasischke et al. (2002)	Up-Valley	263	Higuera et al. (2011)
	Nulato Hills	306*		Down-valley	142	
Alaskan Boreal	Porcupine/Upper Yukon (Central)	~100	Yarie (1981)			
	Sites near Fairbanks, and Delta Junction (Central)	70130	Johnstone et al. (2010a); Johnstone et al. (2010b); Johnstone and Kasischke (2005)			
	Kenai Peninsula		Lynch et al. (2002)	Interior Alaska and Kenai Peninsula	198 ± 90	Lynch et al. (2002)
	Yukon river Lowlands	120	Kasischke et al. (2002)	Brooks Range	145	Higuera et al. (2009)
	Kuskokwim Mountains	218				
	Yukon-Tanana Uplands	330				
	Tanana-Kuskokwim Lowlands	178				
	Kobuk Ridges and Valleys	175				
	Davidson Mountains	403				
	North Ogilvie Mountains	112				
	Ray Mountains	109				
	Yukon-Old Crow Basin	81				

Western North America	Darkwoods, British Columbia	~69	Greene and Daniels (2017)			
	Cascade Mountains, Washington	~27	Wright and Agee (2004)			
	Desolation Peak, Washington Coastal type	108-137				
	Desolation Peak, Washington Interior type	~52				
Eastern North America	Quebec – west	~270*	Bouchard et al. (2008)	Maine	≥ 800	Lorimer (1977)
	Quebec – east	>500*				
				Quebec – “Spruce zone”	570	de Lafontaine and Payette (2011)
				Quebec – “Fir zone”	>1000	
	Quebec – Abitibi northwest	418*	Bergeron et al. (2006 post-1940)^	Quebec – Abitibi northwest	189	Bergeron et al. (2006 post-1940)^
	Quebec – Abitibi southwest	388*		Quebec – Abitibi southwest	165	
	Quebec – Abitibi east	418*		Quebec – Abitibi east	141	
	Quebec – Abitibi southeast	2083*		Quebec – Abitibi southeast	257	
	Quebec – Temiscamingue north	2083*		Quebec – Temiscamingue north	220	

	Quebec – Temiscamingue south	2777*		Quebec – Temiscamingue south	313	
	Quebec – Waswanipi	418*		Quebec – Waswanipi	128	
	Quebec – Central Quebec	388*		Quebec – Central Quebec	150	
	Quebec – North Shore	645*		Quebec – North Shore	281	
	Quebec – Gaspésia	488*		Quebec – Gaspésia	161	
	Quebec – northwestern lakeshore	99'	Bergeron (1991)	Quebec – northwestern lakeshore	63'	Bergeron (1991)
	Quebec – northwestern lake island	112'		Quebec – northwestern lake island	74'	
Fennoscandia	Sweden	*	Niklasson and Drakenberg (2001); Niklasson and Granström (2004)	North Sweden	50-150	Niklasson and Granström (2004); Niklasson and Granström (2000)
				Southern Sweden	20	
	Central Sweden	*	Brown and Giesecke (2014)	Central Sweden - Klotjärnen	180	Brown and Giesecke (2014)
				Central Sweden - Holtjärnen	240	
Siberian Plateau	Northern	300	Kharuk et al. (2016); Kharuk et al. (2011)			
	Southern	80				
	Mean (64-71°N)	110				

^ = The reciprocal converted from burn rate (%) (see Van Wagner et al., 2006)

* = Estimates likely effected in some areas by human activity. In such instances Recent Holocene is preferred.

' = Fire cycle

†='Recent' here refers to records that (or have distinct sections that) begin after the end of the Holocene Climate Optima and end near present

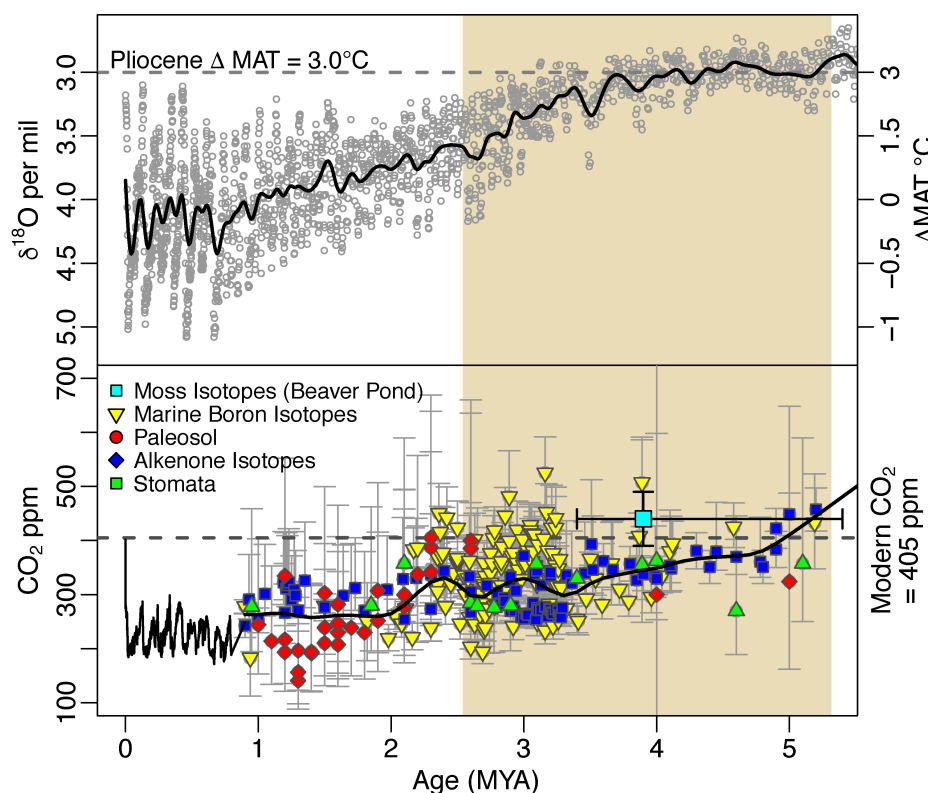




Figure 1: Global temperatures and atmospheric CO₂ concentration spanning the last 5 million years of Earth's history. Mean annual temperatures (MAT) are inferred from compiled $\delta^{18}\text{O}$ foraminifera data (Lisiecki and Raymo, 2005) and plotted as anomalies from present (top panel). Modern atmospheric CO₂ measurements (NOAA/ESRL), and ice core observations from EPICA (Luthi et al., 2008) are compared with proxy estimates (bottom panel; see Table S1) for the Pliocene Epoch indicated with beige shading. Smoothed curves have been fit to highlight trends in $p\text{CO}_2$ and temperature during the Pliocene. The results from this paper (BP) are included with both age and $p\text{CO}_2$ error.

Deleted:  Figure 1. Atmospheric CO₂ concentration and global temperatures and spanning the last 5 million years of Earth's history. Modern atmospheric CO₂ measurements (NOAA/ESRL), and ice core observations from EPICA (Luthi et al., 2008) are compared with proxy estimates (top panel) for the Pliocene Epoch highlighted in red (Hönisch et al., 2009; Pagani et al., 2010; Royer, 2006; Tripathi et al., 2009). Mean annual temperatures (MAT) are inferred from compiled $\delta^{18}\text{O}$ foraminifera data (Lisiecki and Raymo, 2005) and plotted as anomalies from present (bottom panel). Smoothed curves have been fit to highlight trends in $p\text{CO}_2$ and temperature during the Pliocene. The results from this paper (BP) are included with both age and $p\text{CO}_2$ error. 

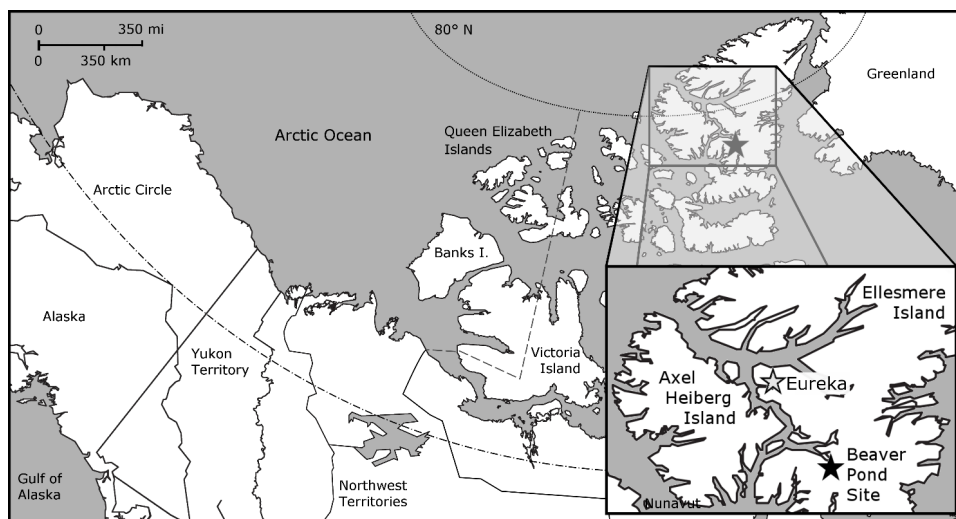


Figure 2. Map of the Canadian Arctic Archipelago, highlighting the location of the Beaver Pond Site (Black Star; 78° 33' N; 82° 25' W) and Eureka Climate Station (Grey Star; 80° 13' N, 86° 11' W – used for modern climate comparison) on west-central Ellesmere Island.

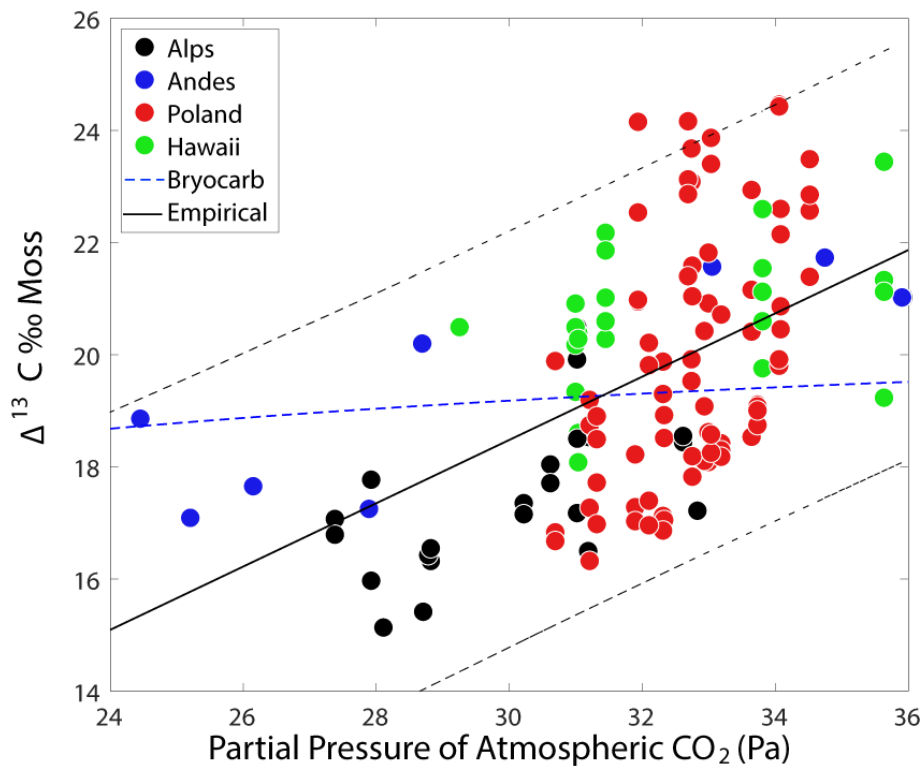


Figure 3. Sensitivity of carbon isotopic discrimination to the partial pressure of atmospheric CO₂ in mosses sampled from different elevational transects. Moss carbon isotope data collected from an elevational transect in the Swiss Alps (black dots; Ménot and Burns, 2001), the Peruvian Andes (blue dots; Royles et al., 2014), the mountains of Poland (red dots; Skrzypek et al. 2007), and Hawaii (green dots; Waite and Sack 2011). Partial pressure of atmospheric CO₂ calculated from atmospheric surface pressure reanalysis data (Dee et al., 2011) combined with atmospheric CO₂ observations from year moss samples were collected. All carbon isotopic measurements of mosses have been normalized to cellulose based on published regression of cellulose and whole moss values (Ménot and Burns, 2001) and reported as discrimination (Δ) from atmospheric δ¹³CO₂ (GlobalView-CO₂, 2013) from the year mosses were collected in units of ‰. Empirical model fit (black line) is plotted with prediction intervals (black dashed) compared with predictions from the BRYOCARB model (Fletcher et al. 2008) with parameters optimized to match observations.

Deleted: two

Deleted: and from an elevational transect in

Deleted: C

Deleted: the natural logarithm of isotopic

Deleted: per mille (i.e.

Deleted:)

Deleted: Optimal model fit (black line) with ± 1σ confidence limits (black dashed lines) from Eq. (9).

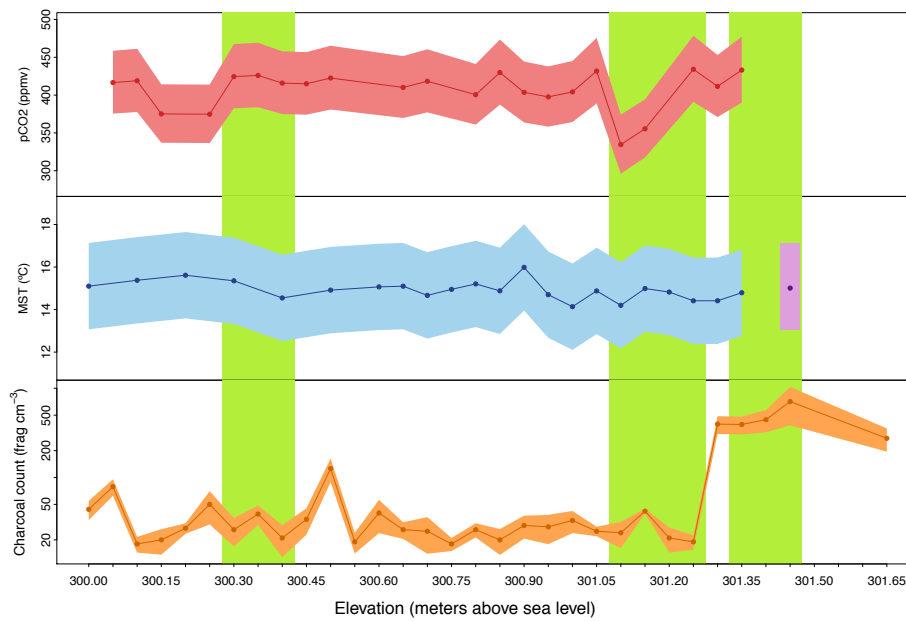
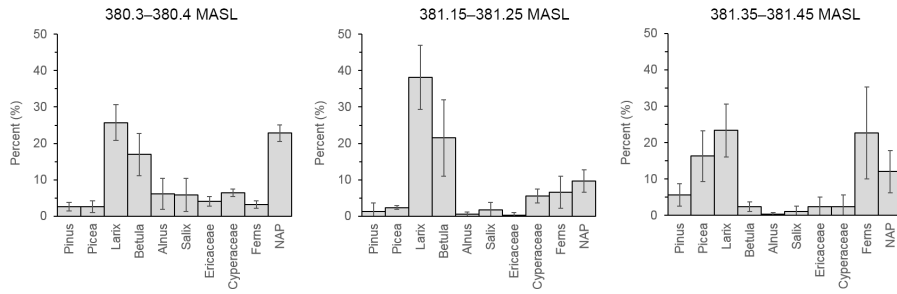


Figure 4. Reconstruction of atmospheric CO₂, mean summer temperature, and fire for the Canadian High Arctic during the Pliocene. Atmospheric CO₂ concentrations estimated from carbon isotopic measurements of mosses and plants (red; $\pm 2 \sigma$). Mean summer temperature reconstructed from a brGDGT based proxy (blue; $\pm 2 \sigma$) and relative 2010 data point in approximate relative position (purple; $\pm 2 \sigma$). Charcoal counts reported as the number of fragments per volume (fragments cm⁻³) of peat (Orange $\pm 2 \sigma$). Green boxes indicate relative depths of pollen sampling. Elevation of the deposit is reported as meters above sea level. (Data: Table S2)

Deleted: from the 2006 series unless noted

(A)



(B)

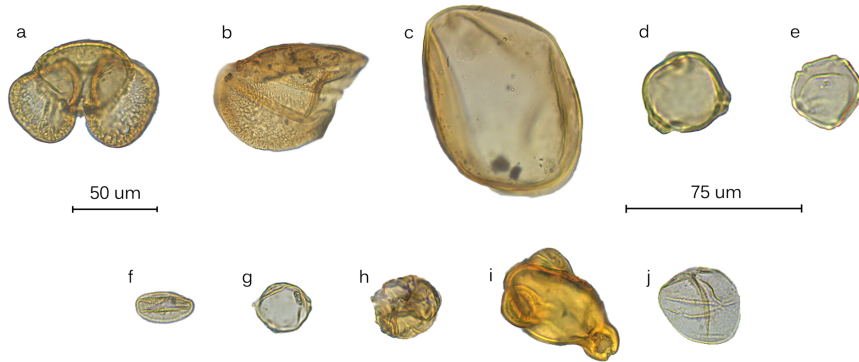


Figure 5. (A) Bar charts showing the relative pollen abundance in each portion of the section (error bars = 95% confidence intervals; MASL- Meters Above Sea Level). (B). Pollen plate of select grains encountered in the BP section: (a) *Pinus*, (b) half a *Picea* grain, (c) *Larix*, (d) *Betula*, (e) *Alnus*, (f) *Salix*, (g) *Myrica*, (h) ericaceous grain, (i) *Epilobium*, and (j) *Cyperaceae*. 50um scale = (a–c), 75um scale = (d–j).

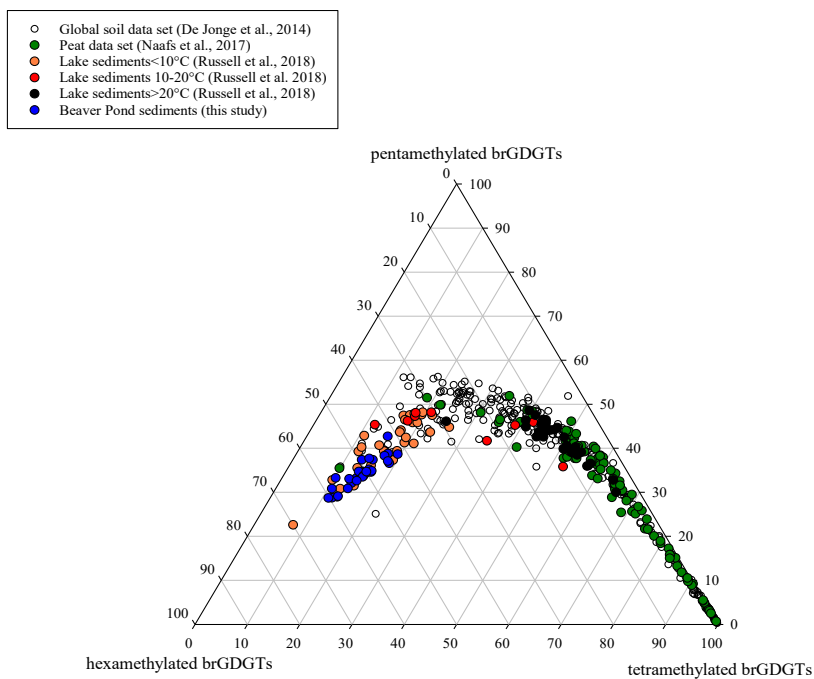


Figure 6. A ternary plot illustrating the fractional abundances of the tetra- (Ia-c), penta (IIa-c and II'a-c), and hexamethylated (IIIa-c and III'a-c) brGDGTs. The global soil dataset (open circles; De Jonge et al., 2014), the global peat samples (green circles; Naafs et al., 2017), and lake sediments from East Africa (black circles indicate samples from lakes >20°C, red circles indicate samples from lakes between 10–20°C and orange circles designate samples from lakes <10°C; Russell et al., 2018) are included for comparison with the Beaver Pond sediments (blue circles; this study).

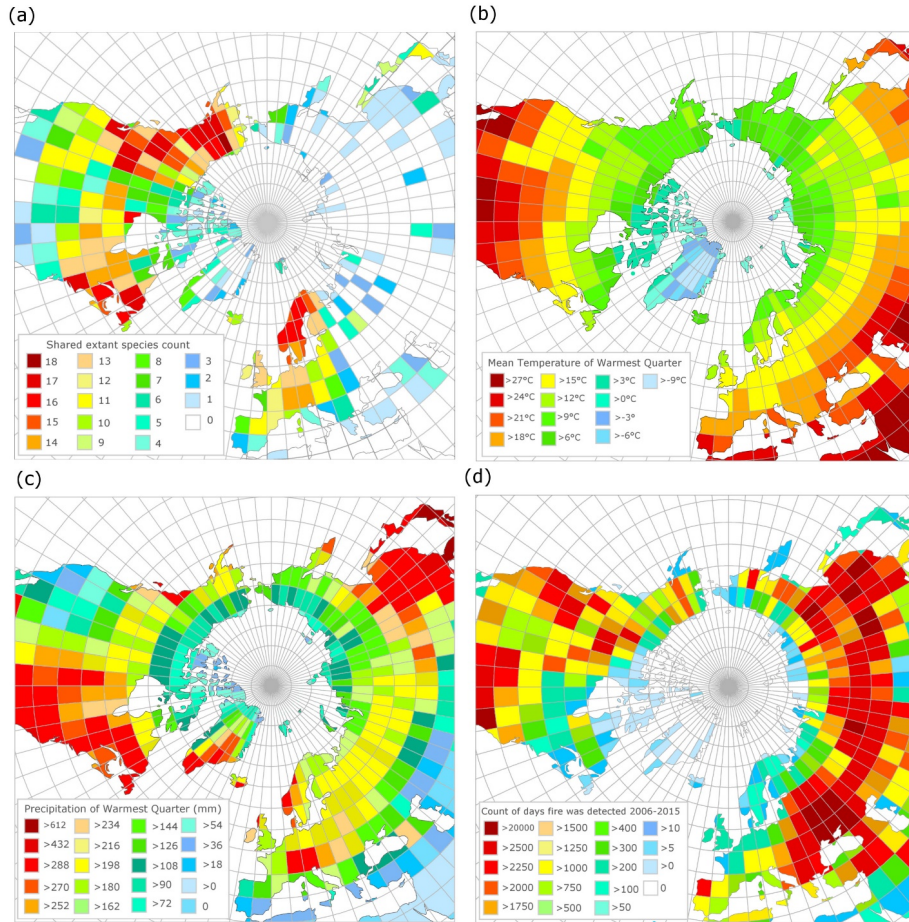


Figure 7. (a) Modern geographic distribution of observed occurrences of species common to the Beaver Pond species list, (b) Mean temperature of the warmest quarter (summer average) derived from WorldClim, (c) Mean precipitation of the warmest quarter (summer rain) derived from WorldClim, (d) Count of unique fire pixels detected per day, over 10 years from MODIS 6 Fire Product, normalized by area of the latitude by longitude grid.

Supplementary Information

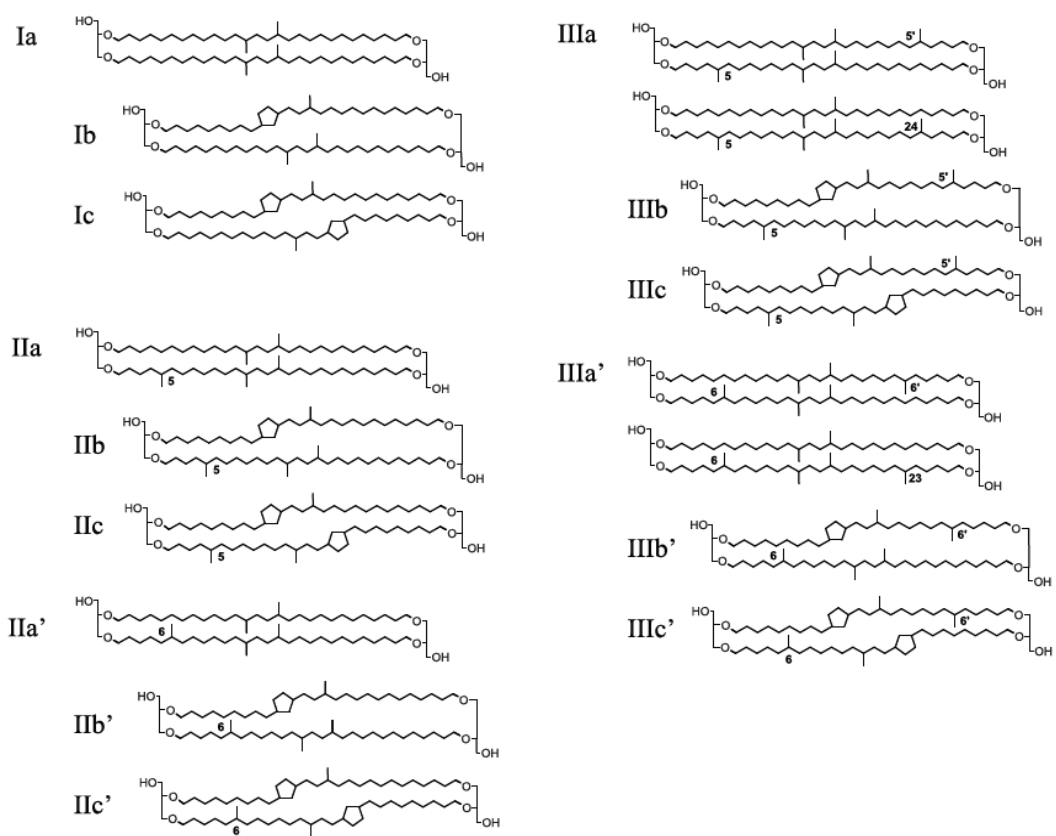


Figure S1. Molecular structures of all 15 brGDGTs (I-III). The molecules designated with a prime symbol are referred to as the 6-methyl brGDGTs.

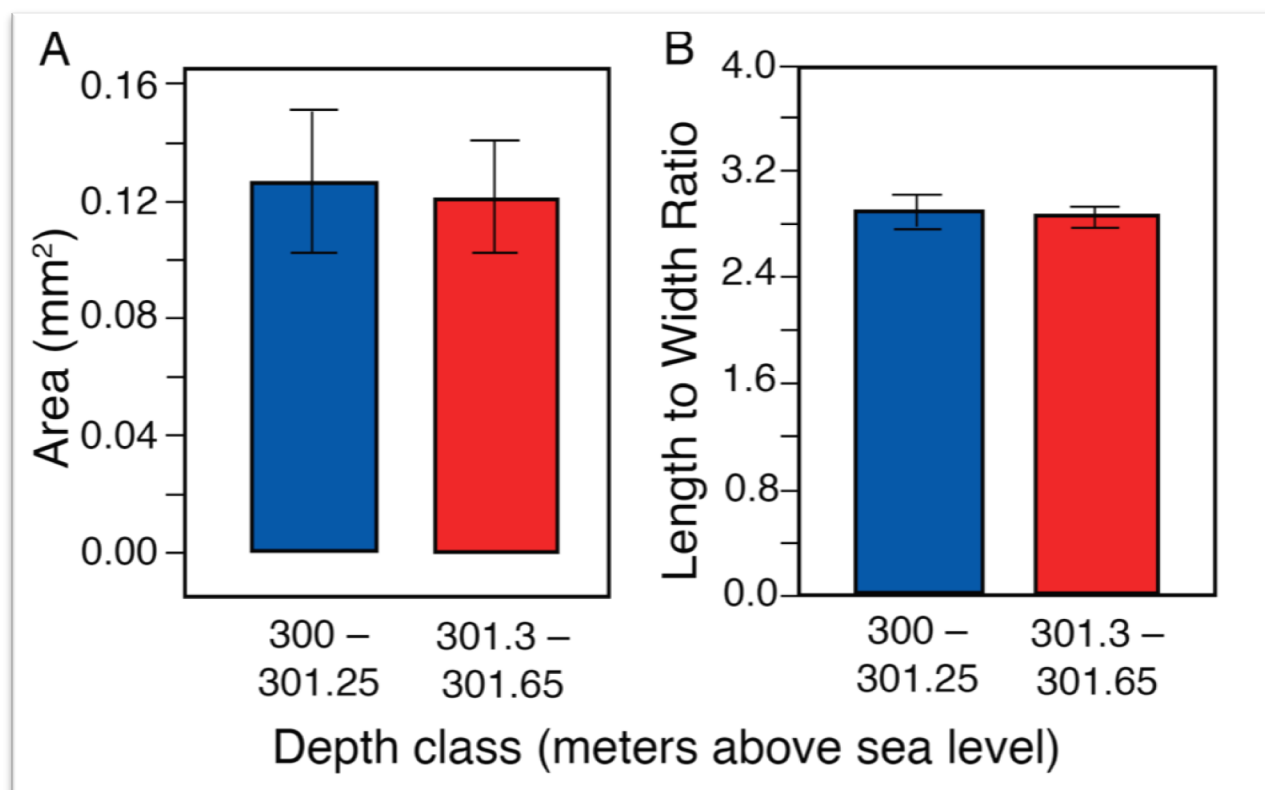
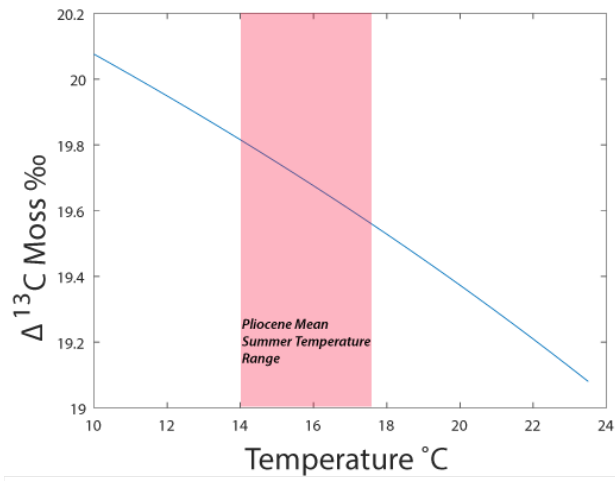


Figure S2. A comparison of the (A) area and (B) shape (length to width) of the uppermost samples (130–165) that have a higher mean charcoal concentration, and the lowermost samples (0–125)

A)



B)

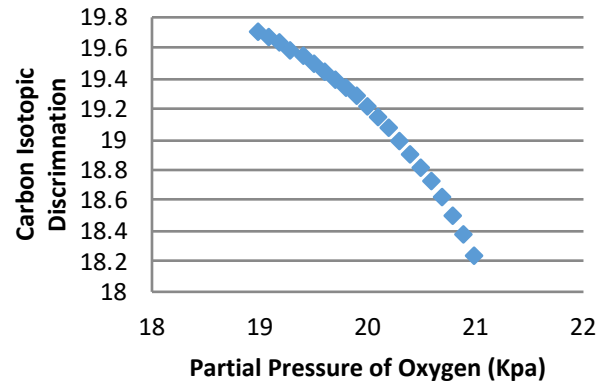


Figure S3. A) Changes in moss $\Delta^{13}\text{C}$ as a function of temperature. Where the entire range of temperatures represents the lapse rate of moss samples from the Peruvian Andes and the red box represents the mean summer temperature range for the Arctic derived from our tetraether measurements. B) Changes in moss $\Delta^{13}\text{C}$ only as a function of $p\text{O}_2$ showing an increase in $\Delta^{13}\text{C}$ with elevation (i.e. reduced $p\text{O}_2$).

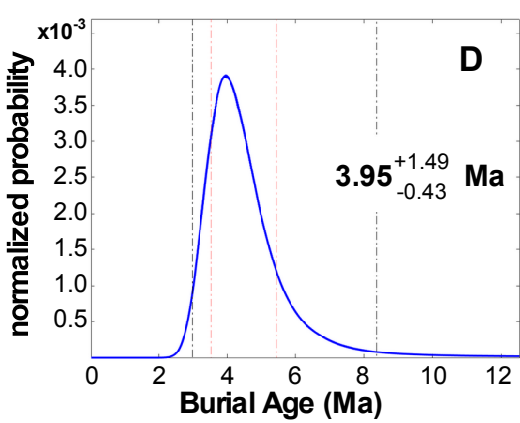
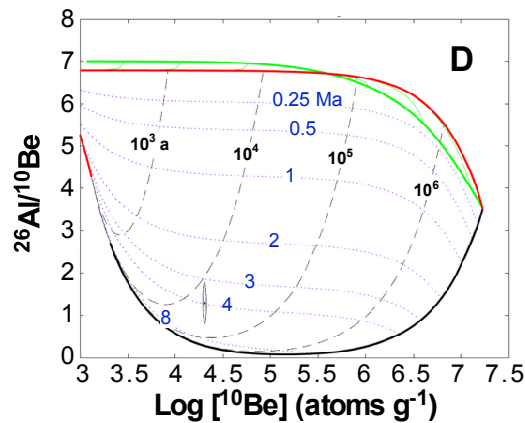
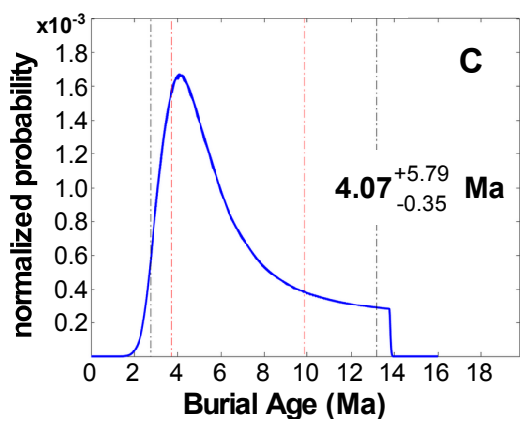
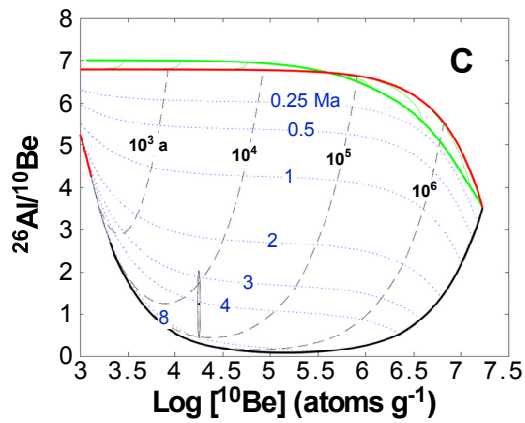
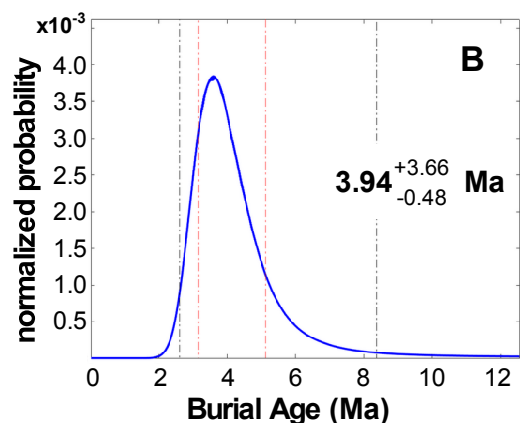
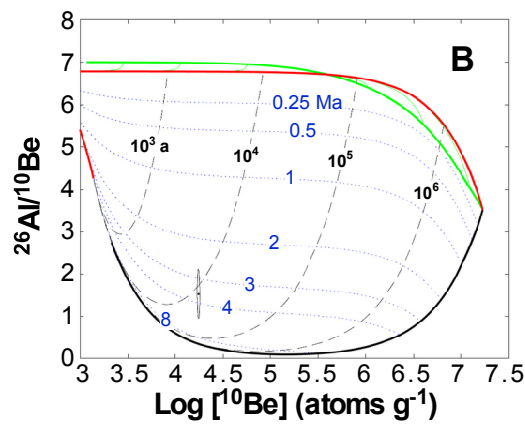
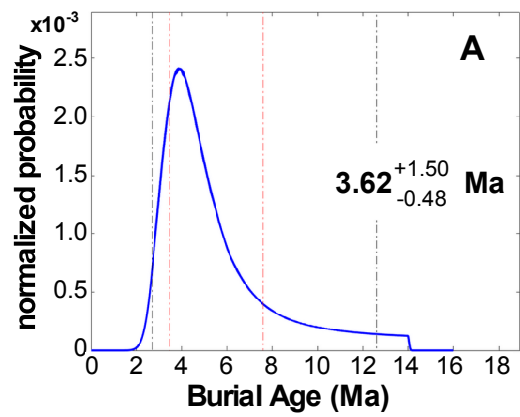
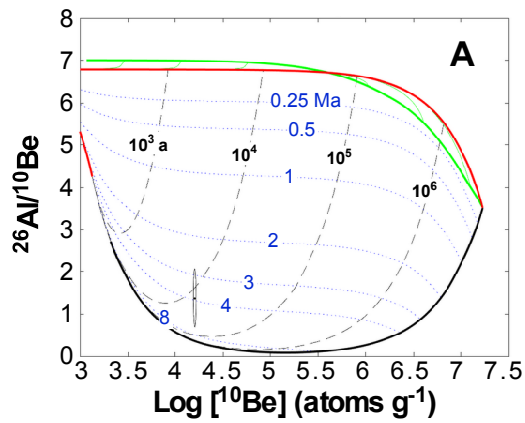


Figure S4. Burial age results. depthID: average initial sample depth, pdfmaxage: the most probable age as determined from the probability density function, sigma1plus and sigma1minus: the $\pm 1\sigma$ errors in pdfmaxage, sigma2plus and sigma2minus: the $\pm 2\sigma$ errors in pdfmaxage, exposure_meanvalue: mean value of pre-buildup exposure age taken from FMINLBFGS optimization algorithm, burial_meanvalue: mean value of burial age taken from FMINLBFGS optimization algorithm. The $^{26}\text{Al}/^{10}\text{Be}$ vs. $\log_{10} 10\text{Be}$ plots are unique for each mass depth. The generally horizontal dotted curves are burial isochrons, from top to bottom 0.25, 0.50, 1.0, 2.0, 3.0, 4.0, and 8.0 Ma, and the near-vertical dashed lines are pre-burial minimum exposure duration isochrons, from left to right 103, 104, 105, and 106 years. The PDF plots are probability distributions of 2000 solutions of the data.

Table S1. Fractional abundances of the brGDGTs found in the Beaver Pond sediments.

Sample Name	Ia	Ib	Ic	IIa	IIb	IIc	IIIa	IIIb	IIIc	IIa'	IIb'	IIc'	IIIa'	IIIb'	IIIc'
BP-A-02	0.08	0.05	0.01	0.15	0.05	0.00	0.27	0.01	0.00	0.12	0.05	0.00	0.21	0.01	0.00
BP-A-03	0.07	0.03	0.00	0.11	0.03	0.00	0.26	0.00	0.00	0.15	0.05	0.00	0.30	0.01	0.00
BP-A-04	0.12	0.04	0.00	0.13	0.03	0.00	0.23	0.00	0.00	0.15	0.04	0.00	0.25	0.01	0.00
06BP01	0.10	0.04	0.01	0.13	0.03	0.00	0.31	0.00	0.00	0.12	0.03	0.00	0.22	0.00	0.00
06BP16	0.11	0.04	0.00	0.15	0.03	0.00	0.30	0.00	0.00	0.13	0.03	0.00	0.20	0.00	0.00
06BP18*	0.11	0.03	0.00	0.15	0.02	0.00	0.29	0.00	0.00	0.14	0.03	0.00	0.21	0.00	0.00
06BP18*	0.11	0.03	0.00	0.15	0.02	0.00	0.29	0.00	0.00	0.13	0.03	0.00	0.21	0.00	0.00
BP-F-73*	0.10	0.04	0.00	0.19	0.03	0.00	0.26	0.00	0.00	0.14	0.03	0.00	0.19	0.01	0.00
BP-F-73*	0.11	0.05	0.00	0.22	0.04	0.00	0.21	0.00	0.00	0.16	0.04	0.00	0.15	0.01	0.00
BP-A-06	0.11	0.04	0.01	0.15	0.03	0.00	0.24	0.00	0.00	0.15	0.04	0.00	0.22	0.01	0.00
BP-A-07	0.13	0.04	0.01	0.16	0.03	0.00	0.23	0.00	0.00	0.15	0.04	0.00	0.20	0.01	0.00
06BP03	0.11	0.04	0.00	0.15	0.03	0.00	0.28	0.00	0.00	0.13	0.03	0.00	0.22	0.01	0.00
06BP05*	0.10	0.04	0.00	0.15	0.03	0.00	0.29	0.00	0.00	0.12	0.03	0.00	0.23	0.01	0.00
06BP05*	0.11	0.04	0.01	0.16	0.03	0.00	0.28	0.00	0.00	0.13	0.03	0.00	0.19	0.00	0.00
06BP07	0.13	0.04	0.00	0.19	0.03	0.00	0.28	0.00	0.00	0.13	0.03	0.00	0.16	0.00	0.00
06BP09	0.09	0.03	0.00	0.14	0.03	0.00	0.30	0.00	0.00	0.13	0.03	0.00	0.23	0.01	0.00
06BP11*	0.11	0.04	0.01	0.16	0.03	0.00	0.31	0.00	0.00	0.12	0.03	0.00	0.19	0.00	0.00
06BP11*	0.10	0.04	0.00	0.15	0.03	0.00	0.29	0.00	0.00	0.14	0.03	0.00	0.21	0.00	0.00
06BP13	0.11	0.04	0.00	0.15	0.03	0.00	0.30	0.00	0.00	0.13	0.03	0.00	0.20	0.00	0.00
06BP14*	0.10	0.04	0.00	0.15	0.03	0.00	0.29	0.00	0.00	0.13	0.03	0.00	0.21	0.00	0.00
06BP14*	0.10	0.04	0.00	0.14	0.03	0.00	0.30	0.00	0.00	0.14	0.03	0.00	0.21	0.01	0.00
06BP15*	0.10	0.03	0.00	0.12	0.03	0.00	0.31	0.00	0.00	0.12	0.03	0.00	0.23	0.00	0.00
06BP15*	0.09	0.04	0.01	0.15	0.03	0.00	0.35	0.00	0.00	0.11	0.02	0.00	0.20	0.00	0.00
06BP17*	0.09	0.03	0.00	0.14	0.03	0.00	0.31	0.00	0.00	0.15	0.04	0.00	0.20	0.00	0.00
06BP17*	0.10	0.04	0.01	0.15	0.03	0.00	0.29	0.00	0.00	0.12	0.03	0.00	0.21	0.00	0.00
06BP19	0.11	0.04	0.00	0.14	0.03	0.00	0.28	0.00	0.00	0.13	0.03	0.00	0.22	0.00	0.00
06BP20	0.11	0.03	0.00	0.16	0.03	0.00	0.30	0.00	0.00	0.12	0.03	0.00	0.20	0.00	0.00
06BP21	0.08	0.04	0.01	0.14	0.03	0.00	0.38	0.00	0.00	0.09	0.02	0.00	0.19	0.00	0.00
06BP22*	0.12	0.04	0.00	0.17	0.03	0.00	0.29	0.00	0.00	0.12	0.03	0.00	0.19	0.00	0.00
06BP22*	0.11	0.04	0.00	0.16	0.03	0.00	0.31	0.00	0.00	0.12	0.03	0.00	0.19	0.00	0.00
06BP23*	0.15	0.04	0.01	0.21	0.03	0.00	0.37	0.00	0.00	0.14	0.03	0.00	0.00	0.00	0.00
06BP23*	0.12	0.04	0.00	0.17	0.03	0.00	0.30	0.00	0.00	0.12	0.03	0.00	0.18	0.00	0.00
BP-F-78*	0.09	0.04	0.00	0.13	0.03	0.00	0.26	0.00	0.00	0.14	0.04	0.00	0.24	0.01	0.00
BP-F-78*	0.10	0.05	0.00	0.15	0.04	0.00	0.22	0.00	0.00	0.17	0.04	0.00	0.20	0.01	0.00

06BP24*	0.12	0.04	0.00	0.17	0.03	0.00	0.30	0.00	0.00	0.12	0.03	0.00	0.18	0.00	0.00
06BP24*	0.13	0.03	0.00	0.16	0.02	0.00	0.28	0.00	0.00	0.13	0.03	0.00	0.20	0.00	0.00
BP-A-16	0.13	0.05	0.01	0.14	0.03	0.00	0.23	0.00	0.00	0.15	0.04	0.00	0.20	0.01	0.00
06BP25*	0.12	0.03	0.00	0.16	0.02	0.00	0.28	0.00	0.00	0.13	0.03	0.00	0.21	0.00	0.00
06BP25*	0.12	0.03	0.00	0.16	0.02	0.00	0.29	0.00	0.00	0.13	0.03	0.00	0.20	0.00	0.00
BP-A-17	0.14	0.04	0.01	0.16	0.03	0.00	0.26	0.00	0.00	0.14	0.03	0.00	0.18	0.00	0.00
06BP26*	0.10	0.03	0.00	0.15	0.03	0.00	0.34	0.00	0.00	0.11	0.02	0.00	0.20	0.00	0.00
06BP26*	0.12	0.03	0.00	0.16	0.02	0.00	0.30	0.00	0.00	0.12	0.03	0.00	0.20	0.00	0.00
06BP27*	0.08	0.03	0.00	0.12	0.02	0.00	0.33	0.00	0.00	0.11	0.03	0.00	0.25	0.00	0.00
06BP27*	0.08	0.03	0.00	0.12	0.02	0.00	0.33	0.00	0.00	0.12	0.03	0.00	0.26	0.00	0.00
BP-A-18 1	0.15	0.04	0.00	0.18	0.03	0.00	0.24	0.00	0.00	0.14	0.03	0.00	0.17	0.00	0.00
06BP28*	0.06	0.02	0.00	0.08	0.02	0.01	0.33	0.00	0.00	0.10	0.03	0.01	0.32	0.01	0.00
06BP28*	0.08	0.03	0.00	0.09	0.02	0.00	0.29	0.01	0.00	0.13	0.04	0.00	0.31	0.00	0.00
06BP28*	0.08	0.03	0.00	0.10	0.03	0.00	0.30	0.01	0.00	0.13	0.04	0.00	0.28	0.00	0.00
BP-A-20*	0.07	0.03	0.00	0.10	0.03	0.00	0.31	0.01	0.00	0.11	0.05	0.00	0.28	0.01	0.00
BP-A-20*	0.08	0.03	0.00	0.11	0.03	0.00	0.29	0.01	0.00	0.12	0.05	0.00	0.26	0.01	0.00
BP-A-69*	0.08	0.04	0.00	0.13	0.03	0.00	0.35	0.00	0.00	0.10	0.02	0.00	0.23	0.00	0.00
BP-A-69*	0.09	0.04	0.00	0.14	0.03	0.00	0.32	0.01	0.00	0.11	0.02	0.00	0.23	0.00	0.00

*indicates polar fraction was re-analyzed

Table S2. Data used to generate Figure 4.

Sample	Elevation	pco2	pco2min	pco2max	MST	MSTmin	MSTmax	CharCount	Charmin	Charmax	1 std	Pollen
06BP01	300				15.10	13.07	17.13	44.00	33.31	54.69	10.69	
06BP02	300.1	417	376	459				79.00	62.44	95.56	16.56	
06BP03	300.1	419	378	461	15.38	13.35	17.41	18.00	14.39	21.61	3.61	
06BP04	300.2	375	337	414				20.00	13.65	26.35	6.35	
06BP05	300.2				15.61	13.58	17.64	27.00	23.39	30.61	3.61	
06BP06	300.3	375	337	414				50.00	29.79	70.21	20.21	
06BP07	300.3				15.35	13.32	17.38	26.00	16.93	35.07	9.07	1
06BP08	300.4	425	383	467				39.00	29.36	48.64	9.64	1
06BP09	300.4	426	384	469	14.55	12.52	16.58	21.00	12.81	29.19	8.19	1
06BP10	300.5	416	375	458				34.00	22.85	45.15	11.15	
06BP11	300.5	415	374	457	14.91	12.88	16.94	126.00	88.73	163.27	37.27	
06BP12	300.6	423	381	465				19.00	14.07	23.93	4.93	
06BP13	300.6				15.07	13.04	17.10	40.00	23.80	56.20	16.20	
06BP14	300.7	410	370	452	15.10	13.07	17.13	26.00	20.49	31.51	5.51	
06BP15	300.7	418	377	461	14.67	12.64	16.70	25.00	13.98	36.02	11.02	
06BP16	300.8				14.95	12.92	16.98	18.00	15.00	21.00	3.00	
06BP17	300.8	401	361	441	15.21	13.18	17.24	26.00	21.27	30.73	4.73	
06BP18	300.9	430	387	473	14.88	12.85	16.91	20.00	13.57	26.43	6.43	
06BP19	300.9	404	364	444	15.98	13.95	18.01	29.00	20.67	37.33	8.33	
06BP20	301	398	358	438	14.70	12.67	16.73	28.00	17.88	38.12	10.12	
06BP21	301	404	364	445	14.14	12.11	16.17	33.00	23.83	42.17	9.17	
06BP22	301.1	432	389	476	14.88	12.85	16.91	25.00	21.94	28.06	3.06	
06BP23	301.1	335	296	374	14.20	12.17	16.23	24.00	16.19	31.81	7.81	
06BP24	301.2	355	318	394	14.99	12.96	17.02	42.00	39.35	44.65	2.65	1
06BP25	301.2				14.82	12.79	16.85	21.00	14.44	27.56	6.56	1
06BP26	301.3	434	391	478	14.41	12.38	16.44	19.00	15.49	22.51	3.51	1

06BP27	301.3	412	371	453	14.41	12.38	16.44	397.00	307.28	486.72	89.72	
06BP28	301.4	433	390	477	14.79	12.76	16.82	393.00	304.74	481.26	88.26	1
06BP29	301.4							445.00	320.14	569.86	124.86	1
06BP30	301.5							710.00	385.49	1034.51	324.51	1
06BP34	301.7							275.00	195.00	355.00	80.00	
BP-A-20*	~301.35				15.01	12.98	17.04					

*2010 field season sample

Table S3. $^{26}\text{Al}/^{10}\text{Be}$ burial ages

PDF max age (yr)	1s error +ve (yr)	1s error -ve (yr)	meanvalue (yr)
3.62E+06	1.50E+06	4.78E+05	3.58E+06
3.94E+06	3.66E+06	4.77E+05	NA
4.07E+06	5.79E+06	3.51E+05	NA
3.95E+06	1.49E+06	4.31E+05	3.95E+06

Table S4. Input for burial modeling

Depth	Bulk	Latitude	Longitude	Surface	^{10}Be conc	^{10}Be conc	^{26}Al conc	^{26}Al conc	Eros
	Density			elevation		err		err	Rate
cm	g cm^{-3}	deg	deg	m	atoms g^{-1}	atoms g^{-1}	atoms g^{-1}	atoms g^{-1}	cm ka^{-1}
18050	2.2	78.550	-82.373	333	17665	402	26986	7335	2.25
18097	2.2	78.550	-82.373	333	16163	376	22263	7889	2.25
18155	2.2	78.550	-82.373	333	17853	387	22322	10215	2.25
18222	2.2	78.550	-82.373	333	20505	598	26508	7147	2.25

Notes:

1. We attempted a depth-profile type isochron burial date (Balco and Rovey, 2010), however the differences in the measured concentrations were too small and uncertainties in ^{26}Al were too large to define an isochron curve. Therefore we used the more common method of simple burial dating using the relationship of $^{26}\text{Al}/^{10}\text{Be}$ vs. $\log^{10}\text{Be}$, which requires the assumption that the pre-burial ratio of the sand samples was the production ratio of $^{26}\text{Al}/^{10}\text{Be}$ (6.75).

2. We computed the $^{26}\text{Al}/^{10}\text{Be}$ burial ages that best fits the measured concentrations, assuming a simple surface buildup and burial history. The depositional environment in the Pliocene was an alluvial fan and pebble-braided-stream system along a mountainous piedmont. Therefore it is reasonable to assume that there was little opportunity for long-term (Ma) deep burial (>20 m) of stored sediment during transport from the nearby mountains. Thus we assume, like most other applications of the simple burial method, that the initial ratio in the sand grains was 6.75 and that only one significant burial event affected the grains in the past 8 Ma (by that time, both isotopes have effectively reached saturation). We use the Lifton et al. (2014) constraints and approach for scaling the production rates in the catchment (buildup) and in the sampled section (post-depositional). The calculations include post-depositional muon production (cosmic ray influx according to Lifton et al., 2014) and erosion of the surface.

3. While the current depth of the samples is approximately 10 m below gravel and till, muons can still penetrate to produce cosmogenic ^{26}Al and ^{10}Be . In other words, the samples are not completely shielded. However, we estimate that there was more sediment and ice above the samples during the Pliocene and Pleistocene as follows: The surface of the Beaufort Formation is more than 40 m higher in elevation across Strathcona Fiord than at BP. Furthermore the region has been significantly eroded since the Pliocene sediment was deposited, as stream paleoflow indicators reveal that the fiord was filled at the time of BP deposition. The amount of erosion in the fiord is much greater than 400 m. We conservatively estimate that 50 m of post-Pliocene erosion occurred above the fiord on the opposite side, or 90 m of sediment loss on the BP side. This would equate to an erosion rate over 4 Ma of 2.25 cm ka^{-1} . Besides sediment with a bulk density of 2.2 g cm^{-3} for coarse sand and sandy gravel, BP would have been covered by ice for the majority of the Quaternary, given its close proximity to the second largest ice field in Canada, Prince of Wales Ice Field. Plateau ice thicknesses are currently >200 m (Kinnard et al., 2008) (i.e. equivalent to approximately 81.8 m of sandy gravel), whereas the ice field is much thicker in valleys and would have been even thicker during much of the Pleistocene. While the mass depth that shielded the samples at any time remains uncertain, our most reasonable estimate is $90.0 + 81.8$ or 171.8 m of average gravel cover (mass depth = $37.8 \times 10^3 \text{ g cm}^2$). We added 171.8 m to each of the modern sample depths (8.70, 9.17, 9.74, and 10.42 m). While the uncertainty in the actual mass depth is large, a greater shielding thickness does not change the age significantly once depths are greater than 50 m (much deeper burial would yield a slightly younger mean age of 3.6 Ma, while a shallower depth estimate will significantly increase the age beyond the ca. 8 Ma saturation limit. Therefore, we prefer the revised calculated mean burial age over the minimum ages reported in Rychczynski et al. (2013) which were derived using unreasonably great depths and zero erosion (needed for no muogenic production) and a superseded production rate systematics.

4. The mean age of the four samples is $3.9 + 1.5/-0.5 \text{ Ma}$. The final most probable ages are therefore our best estimate of burial duration of the Beaver Pond layer. The burial age and error (1σ and 2σ shown in Figure S3) is determined using a systematic parameter search and chi-squared statistic to create a continuous probability density function. We also calculate a burial mean-value age using the FMINLBFGS optimization algorithm (from Matlab file exchange) for comparison

with the probability distribution function most probable burial age approach. Those burial mean-value ages were not available for two of the samples because the tails of their pdfs reach beyond the saturation value.

Supplemental References

Balco, G. and Rovey, C. W.: Absolute chronology for major Pleistocene advances of the Laurentide Ice Sheet, *Geology*, 38, 795–798, 2010.

Kinnard, C., Koerner, R. M., Zdanowicz, C. M., Fisher, D. A., Zheng, J., Sharp, M. J., Nicholson, L., and Lauriol, B.: Stratigraphic analysis of an ice core from the Prince of Wales Icefield, Ellesmere Island, Arctic Canada, using digital image analysis: High-resolution density, past summer warmth reconstruction, and melt effect on ice core solid conductivity, *Journal of Geophysical Research: Atmospheres*, 113, 2008.

Lifton, N., Sato, T., and Dunai, T. J.: Scaling in situ cosmogenic nuclide production rates using analytical approximations to atmospheric cosmic-ray fluxes, *Earth and Planetary Science Letters*, 386, 149–160, 2014.

Rybczynski, N., Gosse, J. C., Richard Harington, C., Wogelius, R. A., Hidy, A. J., and Buckley, M.: Mid-Pliocene warm-period deposits in the High Arctic yield insight into camel evolution, *Nature Communications*, 4, 1–9, 2013.